University of Stavanger

Faculty of Science and Technology

MASTER THESIS

Study program/Specialization: MSc Petroleum Geosciences Engineering	Spring semester, 2016 Open
Writer: Muhammed Mahmoud Abdelrhman Elsheikh	…… (Writer's signature)
Faculty supervisor: Dr. Nestor Cardozo, University of Stavanger	
Thesis title: Mechanical modeling of salt-influenced extensional forced folding	
Credits (ECTS): 30	
Key words: forced folding salt thickness extensional settings strain	Pages: 57 + CD Stavanger, June 15/ 2016

Mechanical modeling of salt-influenced extensional forced folding

by

Muhammed Mahmoud Abdelrhman Elsheikh

MSc Thesis

Presented to the Faculty of Science and Technology

University of Stavanger

University of Stavanger

2016

ACKNOWLEDGEMENTS

I would like to take this opportunity to first thank the almighty God (Allah) who has made this degree possible and for being my strength and guide in the writing of this thesis.

I would like to express my gratitude to my family for their continuous support, motivating and prayers. I would like to thank my thesis advisor Dr. Nestor Cardozo for taking the time to guide me during all the stages of my thesis.

Finally, I would like to thank Dr. Stuart Hardy from the University of Barcelona who kindly provided us with the DEM code to run the simulations.

Abstract

Mechanical modeling of salt-influenced extensional forced folding

Muhammed Mahmoud Abdelrhman Elsheikh
University of Stavanger, 2016

Supervisor: Nestor Cardozo

Scaled and numerical models show that the existence of an evaporite viscous layer (e.g. salt) facilitates the development of extensional forced folds related to basement normal faults. The geometries of the extensional forced folds and the resultant secondary faults are governed by several factors: the thickness and viscosity of the salt layer, the thickness, strength and ductility of the cover sediments, and the amount and rate of displacement on the sub-salt master normal fault. This research focuses on the effect of salt thickness and syn-sedimentation in order to reach a better understanding of the mechanical behavior of salt-influenced forced folding in extensional systems. Twelve 2D mechanical models are generated with three different basement fault dip angles (50°, 60° and 70°). Four models are run for each dip angle in which two of them are run without sedimentation while the other two include growth sediments. Furthermore, a thin and a thick salt layer are considered for each dip angle and syn-sedimentation case. Such modeling process allows us to compare the evolution and related structures of the 12 models. The workflow consists of discrete element modeling (DEM) to simulate normal faulting and forced folding, as well as the computation of total and incremental strain. The study shows that in the presence of a thick salt layer, the decoupling between sub- and supra-salt layers is effective (i.e. the salt efficiently decouples the basement from the overburden

to far extent). For such setting a monocline develops within the cover sediment due to the displacement in the master fault. The forced fold quickly forms and secondary faults develop in the hanging-wall and more in the footwall block of the cover sequence. This geometry resembles an asymmetric triangular zone of faulting initiated at the tip of the basement fault and propagating upwards to the surface. Syn-sedimentation impacts the resultant structures by affecting the evolution of the geometry which is demonstrated by less secondary faults in the footwall and notable decrease in the deformation in the hanging-wall. Understanding the evolution of such faults and deformation styles is important and has wide implications for the exploration and production of hydrocarbons.

Contents

List of figures

1. Introduction

1.1. Background

Thick layers of mechanically ductile weak evaporite (salt) between brittle basement and sedimentary cover units are present in different examples of extensional systems (Paul and Mitra, 2015). The presence of such thick salt layers develops rheological heterogeneity and as a result causes decoupling of the deformation between the shallower supra-salt and deeper sub-salt units which typically result in the development of structural styles that differ notably from those developed in fully brittle systems. For example, due to the decoupling effect of salt, supra-salt monoclines or 'forced folds' and cover-restricted, gravity-driven extensional deformation, may be especially common in salt- influenced extensional settings during the early stages of continental stretching (Lewis et al., 2013).

These differences in structural styles arise basically because of two reasons. First, salt influences the degree of coupling between sub- and supra-salt deformations and secondly activity on sub-salt faults (basement master fault) and supra-salt faults (i.e. faults restricted to cover strata) can generate halokinesis or movement of subsurface salt bodies (Fig. 1). For example, forced folding – which is the main focus of this thesis – above sub-salt normal faults may result in the formation of supra-salt normal fault arrays that may balance basement-involved extension (Jackson and Lewis, 2016).

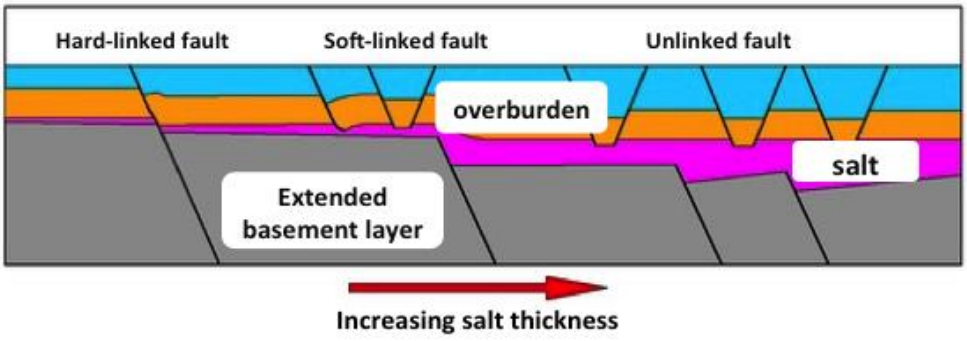

Figure 1. Cartoon showing types of fault linkage depending on thickness of salt layer.

The central focus in this study is to provide a two-dimensional understanding of the mechanical behavior of one of the main factors mentioned previously: salt thickness, which has significant impact on the propagating faults or forced folds in extensional settings. In order to reach this goal, a synthetic workflow is used which is mainly based on geomechanical discrete element modeling (DEM). The discrete element method models the rock material as an assemblage of circular rigid particles in 2D, and its main purpose is to produce a realistic fault geometry and finite strain field (Finch et al., 2004; Hardy, 2011). In addition to varying salt thickness as the main parameter, I look at the impact of syn-sedimentation and dip angle of the basement normal fault.

1.2. Salt-influenced forced folding

An extensive amount of work exists dealing with the formation of buckle folds which are defined as folds formed by compression parallel or at a low angle to the layering or fabric of the rock (Cosgrove, 1999). However, in addition to buckling, there are several mechanisms in the crust that can give rise to folds. One of the most significant mechanisms is forced folding, which has received relatively little consideration. Stearns (1978) defined forced folds as 'folds in which the final overall shape and trend are dominated by the shape of some forcing member below'. In contrast with buckle folds, which are only generated due to layer parallel compression forces, forced folds can be formed in any tectonic regime and equally exist in extensional and compressional systems. Bending is the dominant mechanism during forced folding, which can be defined according to (Cosgrove, 1999) as a flexure of a layer or surface by compressional forces acting at high angle to the layering.

According to (Johnson and Johnson, 2002), efforts to explain forced folds have followed different paths including theoretical analysis, experimentation and kinematic analysis. However, many experimental modeling and seismic analysis have

taken place in relation to salt tectonics in such extensional settings (Lewis et al., 2013). Such studies have shown that the developing structural styles and the degree of coupling between the sub and supra salt deformation is a result of a number of parameters including magnitude and rate of fault displacement, contrast in thickness between the ductile layer and the brittle sediments, physical properties of the salt layers (e.g. density and viscosity), and the degree of differential loading in the overburden (Rowan et al., 2004).

In their study of salt-influenced normal fault growth and forced folding (Lewis et al., 2013) used the Displacement ratio (Dr), which is the ratio between sub-salt fault displacement (D) and original salt thickness (Tv), to predict sub- to supra-salt linkage style (Fig. 2). As a conclusion, they indicated that the single largest control on the style of coupling between sub- and supra-salt normal faults, besides the development of forced folds, is the existence of the salt layer on the sub-salt fault footwall, rather than the absolute thickness of salt. For example, in locations where footwall salt thickness is lower than fault displacement (Dr < 1), a hard-linked or coupled style will form because the hanging wall salt, regardless of its thickness, will be passively translated down the fault surface. In contrast, where footwall salt thickness is larger than fault displacement (Dr > 1), a soft-linked or decoupled style will develop.

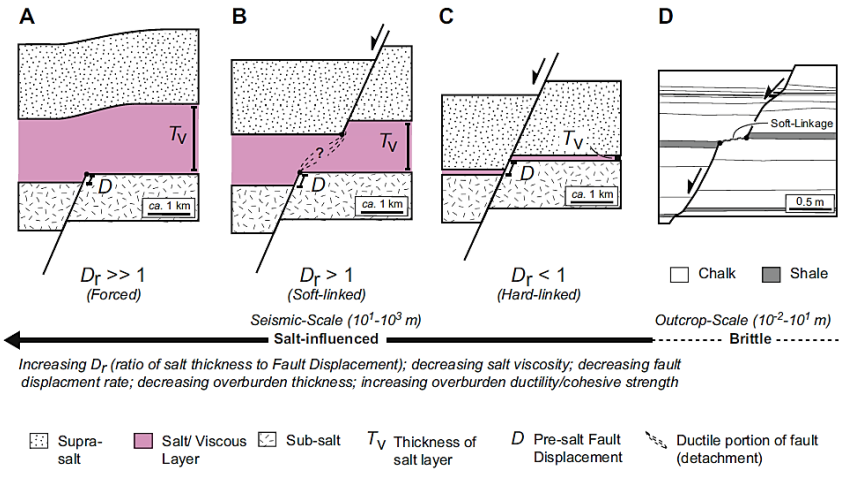

Figure 2. Schematic diagrams illustrating the relationship between the style of sub- and supra-salt fault linkage and the displacement ratio (Dr). Figure D is normal fault growth in brittle systems without salt. From (Lewis et al., 2013).

Studying the effect of salt thickness on the structural styles and associated secondary faults of extensional forced folds is crucial for oil and gas exploration. This is due to the fact that hydrocarbons are commonly trapped within shallow secondary structures and faults related to extensional forced folding and within the underlying fault blocks (Fig. 3); (Withjack and Callaway, 2000). In addition, the existence of evaporitic packages within extensional forced folds significantly affect the quality of the seismic images, due to the difference in densities and velocities between salt and the adjacent layers which in turn leads to low signal to noise ratio and makes seismic interpretation more difficult. Therefore, a better understanding of the deformation patterns and the behavior of salt during extensional forced folding can provide geoscientists with the sufficient guides for interpreting subsurface data of these structures. Specifically, this information can aid exploration and production efforts in extensional salt basins, including the North Sea, the Gulf of Suez, offshore eastern Canada, and the Gulf of Mexico (Withjack and Callaway, 2000).

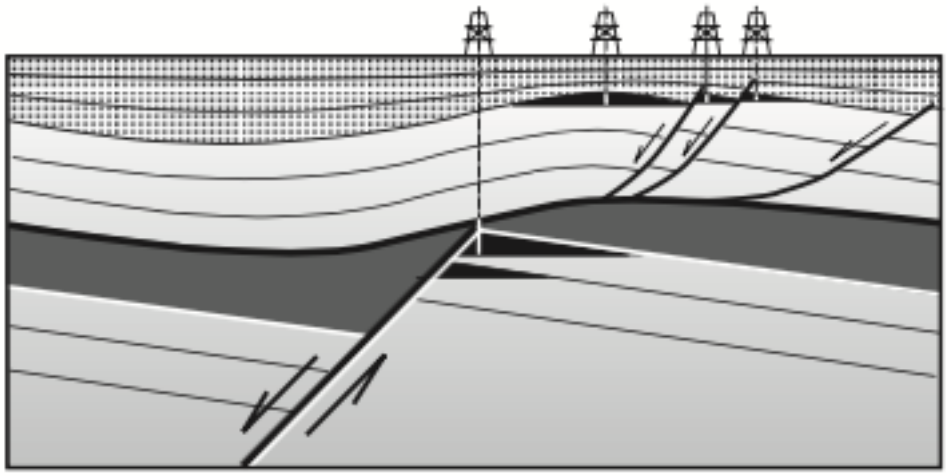

Figure 3. Sketch of an extensional forced fold above a master normal fault. Dark gray layer represents an evaporitic package. Hydrocarbons are trapped within the secondary supra-salt structures produced by the forced folding and within the subsalt fault block, modified from (Withjack and Callaway, 2000).

As mentioned previously, this thesis focuses on the influence of salt thickness as a fundamental parameter in investigating the sedimentary cover deformation above steep basement normal faults. The study approaches this aim by generating a

series of 2D discrete element models to monitor the deformation in the cover sediments through its geometry and strain, similar to the work of Finch et al. (2004; Fig. 4). The salt thickness is varied twice with different dip angles (50°, 60° and 70°) of the basement normal fault. Half of these models include sedimentation in order to explore the impact of growth strata on the deformation style in the cover sediments. In each model, the evolution is examined at different stages of displacement of the master fault. Moreover, finite and incremental strains are computed for all models to image the different fault structures and their activity.

1.3. Thesis objectives

The main objective of this thesis is to gain a more solid understanding of the mechanical behavior of forced folds and related structures that are affected by the presence of salt in basement-involved extensional systems. One important parameter that is considered to have a great impact on the relationship between sub and supra-salt deformation and the resultant structures is salt thickness. In order to investigate its influence, discrete element modeling (DEM) is applied in this study to simulate faulting and forced folding in the cover sedimentary layers with and without growth sedimentation. This is similar to the study of Finch et al. (2004), but in this case we are considering a basal salt layer. By varying salt thickness and run several models we can try answering main questions: to what extent does salt thickness play a role in the deformation between the underlying salt and the overlying brittle formations? And, what is the type of decoupling or fault linkage such parameter may produce?

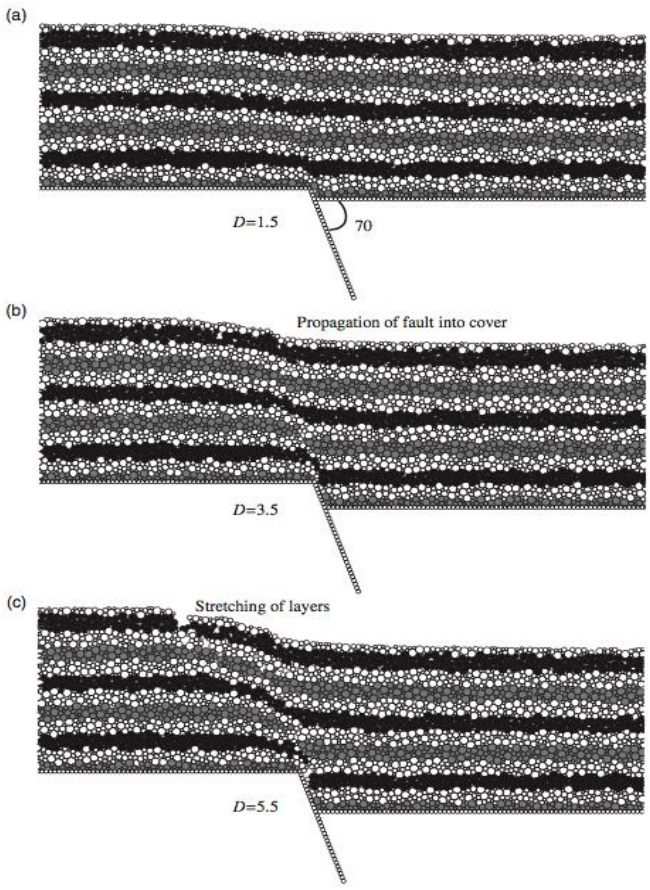

Figure 4. Example of a DEM of extensional forced folding. Results of a 70° basement fault experiment after (a) 1.5, (b) 3.5 and (c) 5.5 units of fault-parallel displacement. The layering is for visualization purposes only (Finch et al., 2004).

2. Methodology

2.1. Overview

The aim of this contribution is to provide a two-dimensional understanding of the mechanical behavior of forced folding that is influenced by the presence of salt in basement-involved extensional settings. To reach that goal, a series of discrete element numerical experiments are conducted in this thesis. 12 models take two variables in consideration: salt thickness and growth sedimentation. For this study, the models are run for three different basement fault dip angles (50°, 60° and 70°). Salt thickness is varied within the models to evaluate its influence on the developing structures.

The approach used in this study includes simulating and modeling the salt-influenced forced folding using cdem2D, which is a computer code for the discrete element model (DEM) developed by Stuart Hardy at ICREA, University of Barcelona. This code is useful and compatible with the resolution of this thesis, where the rock mass is considered as an assemblage of circular particles in 2D (Fig. 5). The particles are rigid with meter-size scale, a given density, and other modeling parameters, which would be explained later in this chapter. Moreover, finite and incremental strains are computed in order to improve our understanding of the deformation. Strain is computed using the computer program SSPX by Cardozo and Allmendinger (2009).

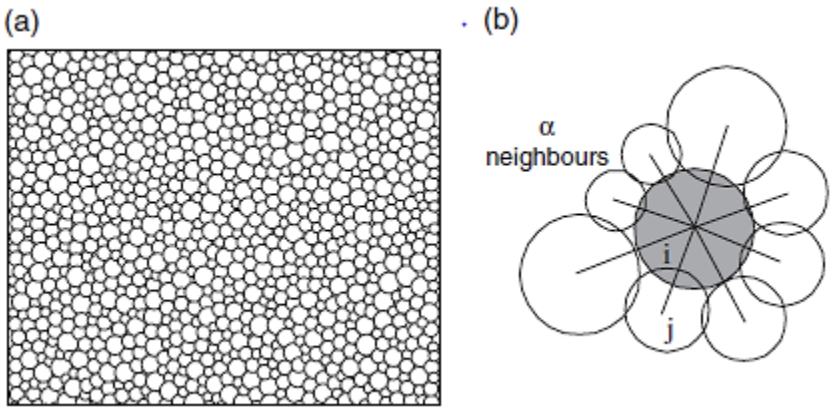

Figure 5. Illustration of the discrete-element technique used in the modelling: (a) packing of particles of four different radii; (b) relationship between a given particle i and its α neighbours, particles interact under gravity, elastic, frictional, and viscous (in the case of salt) forces (Hardy and Finch, 2005).

2.2. Mechanical modeling

2.2.1. Background

The key objective of the mathematical modeling of any physical process is to predict the behavior of an object or system to a realistic level of accuracy. However, the most effective mathematical model is that one which yields the required response to a sufficient accuracy and cost (Bathe, 1996). By averaging the properties of a physical material or environment on the microscopic scale, it is usually possible to model macroscopic behavior. Nevertheless, a reliable model would reduce the necessity for repeated physical testing which is generally costly and subject to experimental error.

Mechanically based numerical modeling is considered as a powerful tool to investigate fundamental processes related to the formation and evolution of large and small-scale geologic structures. A widely used computer modeling technique in the field of mechanics is the Finite Element Method (FEM). This is a robust tool for examining and analyzing the physical mechanics of continuous materials. However, in some applications these methods are not appropriate due to the fact that they need

the system to be represented as continuum. This assumption is not convenient for many physical processes where local discontinuities (e.g. faults) affect the macroscopic behavior of the system. Nonetheless, to overcome such issues several advances in the field of numerical modeling led to the development of the discrete element modeling (DEM) as a discontinuum, numerical method (Fig 6).

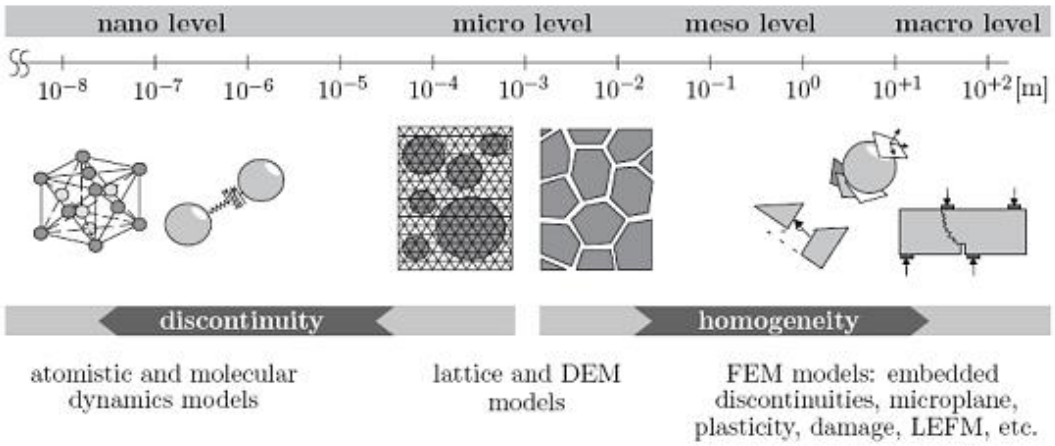

Figure 6. Observation scale in the classification of numerical modeling techniques of materials (D'Addetta, 2004).

According to Hart (1988) a major distinguishing feature of a discontinuum analysis method in comparison with continuum analysis approaches is that the discontinuum method explicitly represents the discontinuities of the rock mass in the numerical formulation. Such feature is very useful when considering modeling of geological features such as faults.

2.2.2. Discrete element modeling

The discrete element modeling is a discontinuum method used to model and simulate the dynamic evolution of a system of discrete elements under applied forces and displacement boundary conditions (Gray et al., 2014). In contrast with continuum techniques, these methods use simple particle interactions and as a result allow the dynamic evolution of a system to be modeled and monitored. In addition, it is an

appropriate technique for examining problems in which discontinuities (faults, joints or fractures) are important. This is mainly due to the fact that it allows deformations involving large relative motion of individual particles, without re-meshing at moderate to high strains (Cundall and Strack, 1979; Hardy and Finch, 2005). Furthermore, discrete element methods permit localization and the formation and linkage of fractures as a regular part of the numerical scheme. Cundall (1971) was the first to use the discrete element method to simulate failure of a system of semi-brittle jointed rock blocks. Since then, extensive work and advance developments of the discrete element method have dealt with problems in soil mechanics and granular media, as well as in chemistry and physics to simulate liquid and gas behaviors (e.g. (Cundall and Strack, 1979; Kuhn, 1999)).

The DEM is not the only possible way to monitor the dynamic evolution of geologic structures and produce a representative image of faults. A digitized and parameterized schematic of a fault based on outcrop data can be sufficient for this purpose as well. However, the outcrop model may not be exempt from problems related to strain heterogeneity and most importantly there is the challenge of upscaling petrophysical properties from the outcrop to the scale of industry standard seismic acquisition at a few kilometers of depth (Botter et al., 2014). Besides producing realistic fault architectures, the DEM also provides flexibility for imposing different displacement and stress boundary conditions, as well as upscaling in terms of a continuous parameter such as strain (Botter et al., 2014).

In the DEM, the rock mass is treated as an assemblage of rigid circular elements, which interact in pairs as if connected by elastic bonds and undergo motion relative to one another (Hardy et al., 2009). These elements interact with elastic, gravitational, frictional and viscous (in the case of salt) forces (Fig. 3). At each discrete time step, the particles are moved to their new positions within the model by integrating their equations of motion using Newtonian laws and a velocity-Verlat-based scheme (Allen and Tildesley, 1987).

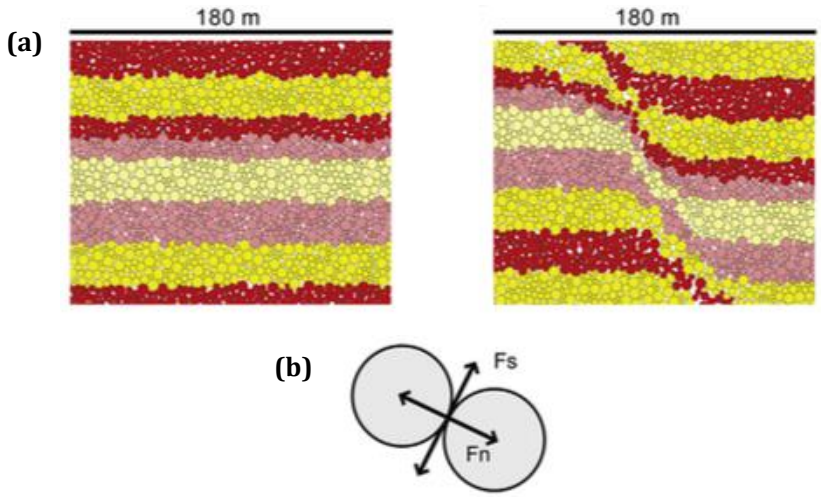

Figure 7. Example of the DEM: (a) Zoom in before and after faulting, initial fault model with four different particle radii and boundary conditions for a 60° dipping normal fault, (b) Normal (Fn) and shear (Fs) forces between particles (Modified from: (Botter et al., 2014))

2.2.3. Advantages and disadvantages of the DEM:

All numerical techniques have advantages and downsides in their application to geological problems. The discrete element method is not an exception (Gray et al., 2014). The advantages and disadvantages of the DEM are summarized as follows:

Advantages:

- In contradiction with the continuum approach, the DEM does not require sophisticated constitutive relations in geomechanical applications,
- A reliable method for simulating the distinct behavior of granular materials,
- Applicable to investigate fracture mechanics, large displacement and large strain problems,
- Because of its fully dynamic nature, it is regarded as efficient in the visual recognition of geologic problems such as faulting and folding.

Disadvantages:

- Extensive and computational time-consuming, therefore it is not practical to simulate large problems,
- In kilometer-scale simulations like the ones in this study, particles are large (meter size), and therefore grain-scale processes are not modeled,
- Requires calibration studies of particle parameters for determination to the emergent rock physical properties,
- Few computer programs relatively available on DEM in the market currently.

On the whole, the DEM is considered to be an appropriate method to study the process of faulting along its different stages of initiation, propagation and linkage, including forced folding and fault-related folding in general.

2.3. Modeling Parameters

2.3.1. Experimental boundary and initial conditions

In this thesis, the discrete-element model is applied to problems related to the development of forced folding influenced by salt in basement-involved extensional setting. In this context, deformation is a result of extensional forces at the base of the model. The particle assembly contains initially 45,000 elements, with different radii ranging between 6.25 m and 15.625 m. This assembly is created with elements positioned at random in an bounded rectangular box and then permitted to relax to a stable equilibrium (i.e., when all particles in the assembly have come to rest and their positions change only insignificantly, and consequently the gravitational potential energy is nearly constant) (Hardy et al., 2009).

The model is divided into 24 layers arranged horizontally above and vertically below. The horizontal layers represent the brittle cover sediments while the vertical ones represent the ductile salt (Fig. 4). In the case of growth strata, new particles are

added to the top of the model after every 20 meters of boundary displacement. That leads to a total of 50 sedimentation steps along the displacement process, at a rate of two layers added at each stage. The initial model parameters are chosen as a result of thorough model tests performed by Stuart Hardy at the University of Barcelona to determine values that are appropriate for the media under consideration. These initial conditions could be summarized as follows:

Number of (initial) assembly elements = 45596
Number of (initial) assembly elements including walls = 46475
Initial model width (m) = 6250.0
Initial model height (m) = 2769.79
Minimum element radius (m) = 6.25
Maximum element radius (m) = 15.625
Average element radius (m) = 9.711104
Boundary/wall element radius (m) = 15.625
Gravitational constant (m/s2) = 9.81
Viscosity (damping) constant (N.s.m-1) = 3.000000E+07
Element Density (kg/m3) = 2500.0
Unit scaling length (m) = 125.0
Total displacement (m) = 1000.0
Fault location (m) = 3125.0
Internal (element-element) Coefficient of friction = 0.35
Boundary displacement (m/s) = -0.1
Boundary displacement (m/time step) = -0.0002
Display/Recording increment (m) of boundary displacement = 1.0
Incremental displacement (m) = 1.0
Total number of output files (including 0 time) = 1001

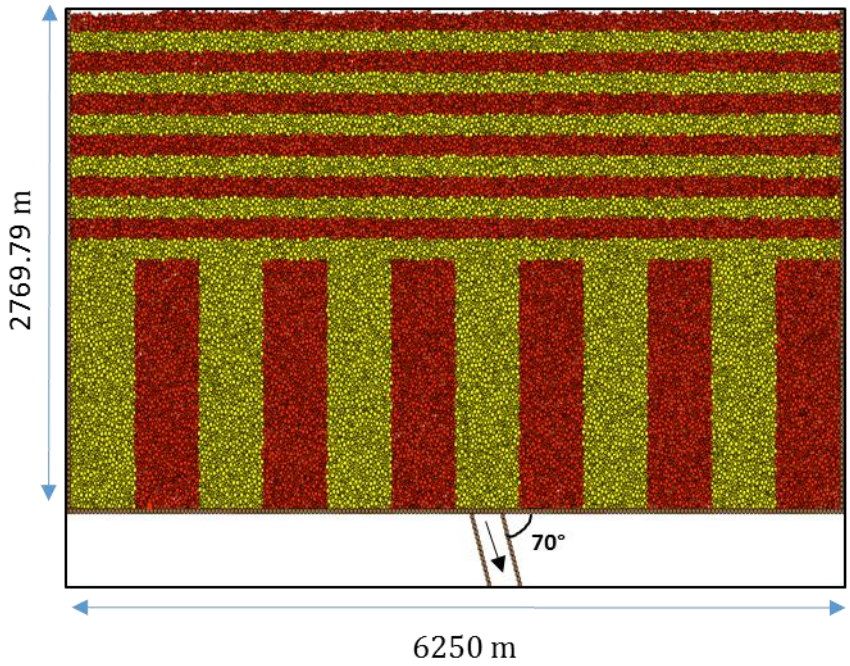

Figure 8. Example of the DEM used in this thesis in the initial condition. The horizontal layers represent the brittle cover sediments while the vertical ones represent the ductile salt. A displacement boundary condition is applied at the base to simulate a 70° dipping normal fault. Total number of elements = 45596.

Notice that the displacement values along the boundary are shown with minus sign (-). This is because of the formulation in which negative displacement values are used for down and towards the right displacement, which express the extension mode. The total number of output files that the code generates is about 1000, with an increment equal to one meter of boundary displacement.

In total, 12 experiments are generated with three different basement fault dip angles (50°, 60° and 70°). Four models represent each dip angle in which two of them are run without sedimentation while the other two include growth sediments. Moreover, salt thickness is varied for each dip angle with and without sedimentation. In half of the models, the thickness of the salt is half the model thickness (i.e. 12 model layers), while in the other models the salt thickness is reduced by half. This allows us to monitor and compare the geometry evolution and related structure styles for thick versus thin salt models.

2.3.2. Strain computation

Discrete element models consist of individual particles of finite size. For this reason, it is essential to establish a link between particle displacement and macro level deformations, as we require to interpret the DEM results from a macro-level perspective (Bagi, 2006). To monitor the geometry and model evolution, and compute strain, the program SSPX is used. SSPX is a Macintosh based software that facilitates the computation of strain and strain rate from displacement/velocity data in 2D and 3D (Cardozo and Allmendinger, 2009).

Strain allows us to see to what extent a material has been deformed, where and when the deformation took place. In our context, it helps to improve our understanding of the geometry evolution and different type of deformation along the modeling process. Finite and incremental strains are computed using Delaunay triangulation. SSPX constructs a mesh of Delaunay triangles with vertices defined by the particles, and then calculates and plots the strain in each triangle. Four results for each experiment are displayed at every 250 m of fault displacement. This allows us to evaluate and express the extensional model as it advances with time and displacement. Figure 5 is an example of the strain computation in one of the model's steps, showing how fundamental strain is for our understanding of deformation and its development along the modeling process.

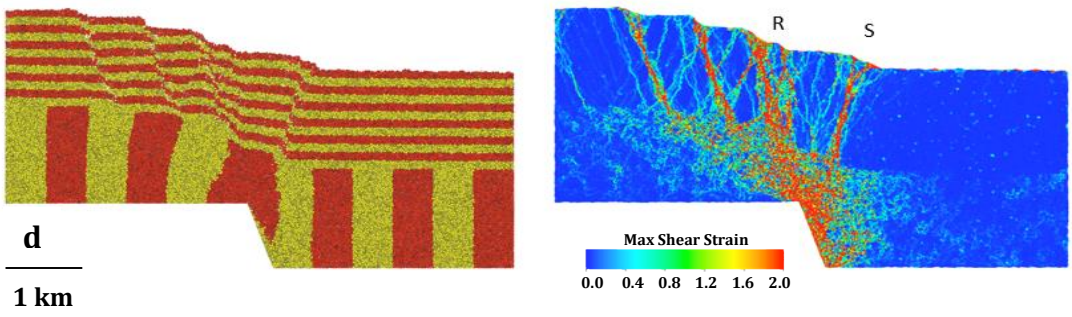

Figure 9. Example of the DEM model of Figure 8 at 1000 m fault displacement. Left is the geometry and right is the finite shear strain. All faults and structures are clearly imaged using the Delaunay strain computation method.

3. Simulation results

In this chapter the influence of salt on deformation and fault linkage is investigated through twelve different simulations. Experiments without growth sedimentation are discussed first while models including syn-sedimentation come later. Both kinds of models are examined with basement normal faults dipping 70°, 60° and 50°. For each dip angle there are two experiments: one with a thick salt layer and another with a thin salt layer. The thick salt layer consists of 12 layers, while the thin salt layers consists of six layers.

As described in the methodology, the total number of output files the code generates is about 1000, with a recording increment equal to one meter of boundary displacement. The results for each model are displayed at 250, 500, 750 and 1000 m of fault displacement, which gives a good summary of the structure's evolution.

3.1. Models without growth strata

3.1.1. 70° dip fault

3.1.1.1. Experiment 1 - thick salt

From the geometry and total shear strain (Fig. 10a), it can be observed that after 250 m of displacement of the basement master fault; a very gentle monocline or forced fold has developed in the cover sediments with a notable steep reverse fault (R). Shear strain is spreading immediately above the basement fault tip and diffusing over the thick layer of salt leading to a fanlike shape through the salt while the incremental shear strain shows that most of the deformation is accommodated by the salt at this stage. The total shear strain also represents a complex zone of steep and curved faults, which are about to develop at the upper edge of the salt layer and propagate upwards, curving into the hanging-wall. The dominant, visible single

reverse fault represents this zone of faulting while several minor normal and reverse faults are still under development and can only be noticed from the shear strain map.

At 500 m with continued displacement, two distinct groups of faults have formed (Fig. 10b). One group consists of reverse faults including the previous fault (R) along with another fault (S) to the right of it. The other group contains three normal faults further towards the footwall with increasing dip angle towards the basement fault tip. The total shear strain shows that the previous curved reverse fault (R) is cut by a steep normal fault that propagates further upwards while the incremental shear strain expresses that still most of the active deformation takes place within the salt layer towards the footwall block.

The next increments of displacement (750 and 1000 m total) exhibit the increase in displacement in the secondary faults, which become well defined both in the footwall and the hanging-wall (Fig. 10c, d). However, the first reverse fault (R) is now essentially inactive as no increase in the displacement is observed from the geometry illustration. The total shear strain shows more deformation in the previous fault groups with evidences for more secondary faults yet to develop. From the incremental shear strain it can be observed that most of the deformation takes place in the footwall block of the cover sediment while the hanging-wall faults (R) and (S) are totally inactive at this stage in addition to an attenuation in the incremental strain/movement of the salt.

In the final stages of master fault growth, it can be noticed how the salt is effective in decoupling the sub- and supra-salt layers as the master fault does not propagate all the way upwards, instead, different type of structures formed in the cover sediments. This has taken place as the salt above the basement flows by thinning in the footwall side and thickening in the hanging-wall for effective decoupling.

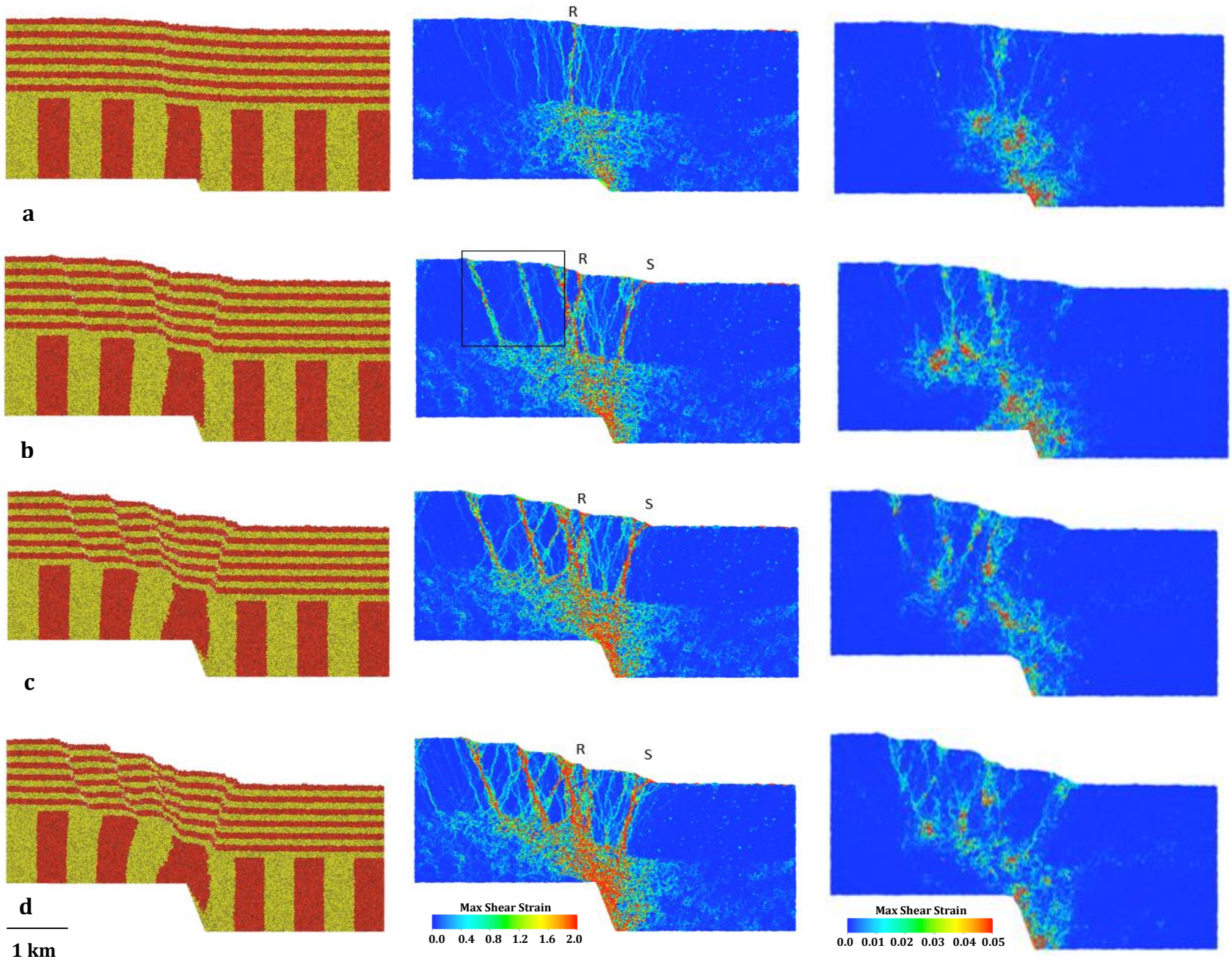

Figure 10. Evolution of model geometry (left) , total strain (middle) and incremental shear strain (right) at (a) 250, (b) 500, (c) 750 and (d) 1000 m basement fault displacement for an experiment with thick salt layer and a basement fault dip of 70° without growth strata.

3.1.1.2. Experiment 2 - thin salt

The geometry and total shear strain (Fig. 11a) show that after 250 m of displacement of the basement master fault a forced fold has clearly developed in the cover sediments with not only a steep reverse fault this time but with normal faults as well. The faults develop above the basement fault tip immediately over the thin salt layer in a narrow zone compared to the previous model. A steep curved reverse fault (R) has formed first in the early stages of extension followed instantly by a normal fault (M) which cuts the former from the middle. Subsequently another normal fault (N) appears with similar dip angle located further towards the footwall. Total shear strain spreads and diffuses over the thin layer of salt leading to a fanlike shape while the incremental strain shows that most of the active deformation at this stage is in the salt.

As the displacement continues, at 500 m the reverse fault (R) becomes essentially inactive while normal faults are more dominant with a remarkable increase in the faulting zone (Fig. 11b). This could be clearly seen from the incremental shear strain. Moreover, from the geometry and total shear strain, it can be seen that the leftmost normal fault (N) is splitting into two or more faults.

The next increment of displacement (750 m) exhibits the increase in displacement in the secondary normal faults in which faulting zone becomes wider with more faults to exist in the footwall (Fig. 11c). Active faulting forces some of the cover beds both in the hanging-wall and footwall to dip towards each other as a result of extension. This time the incremental shear strain shows that large amount of strain is applied through the salt as the normal fault (N) approaches the master fault dip angle.

In the final stage of the master fault growth at 1000 m the leftmost zone of faulting (N) becomes more dominant and approximately dips with the same angle as the master normal fault (Fig. 11d). The incremental shear strain shows almost no active faulting except for the normal fault (N). This - in addition to the previous results - highlights the minor impact of the thin salt layer as an intra-stratal detachment and thus less decoupling between sub- and supra-salt deformations. However, the whole setting is now divided into a well-defined hanging-wall and footwall. The total shear strain shows evidences for more secondary faults yet to develop, which enlarge the zone of deformation.

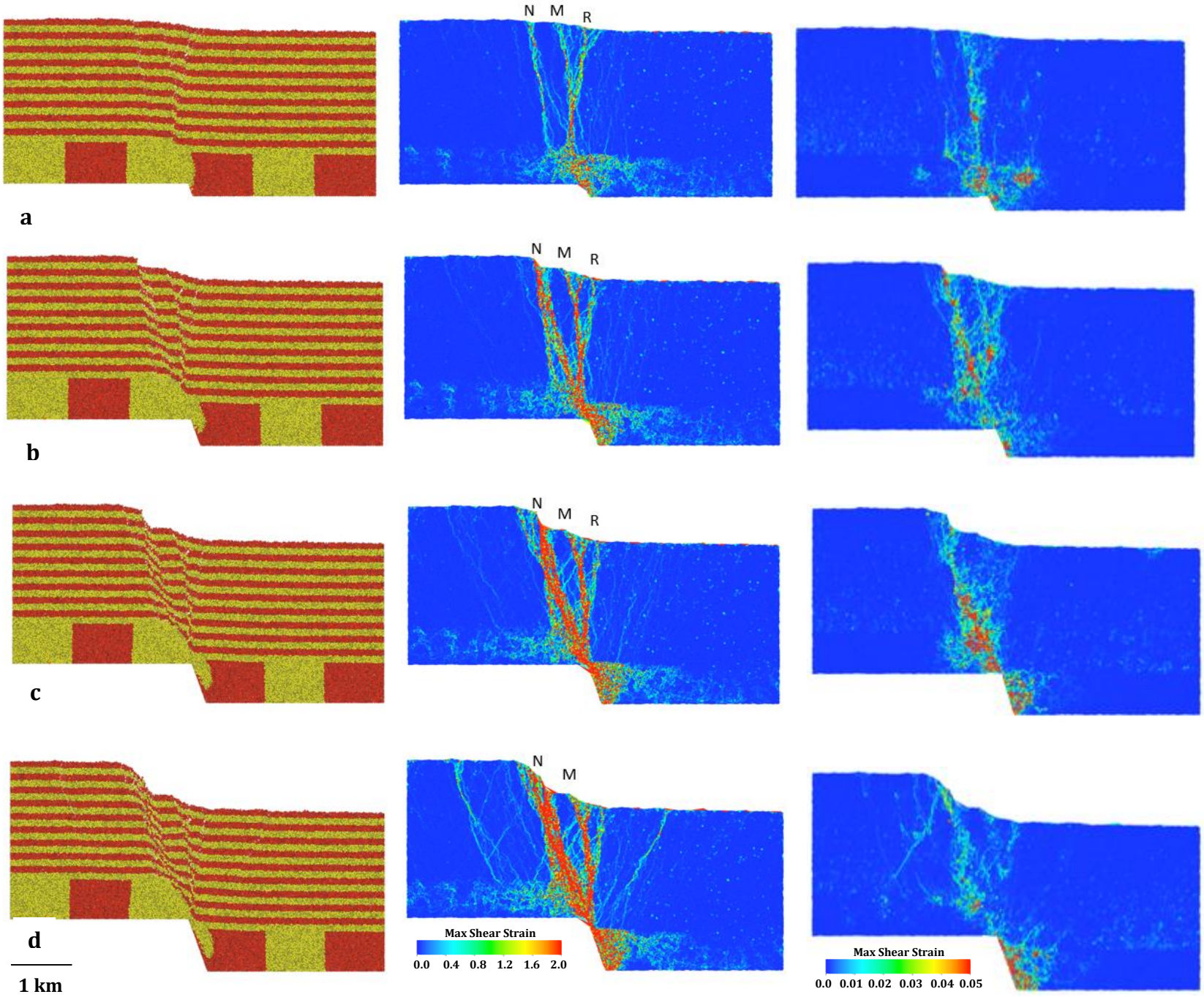

Figure 11. Evolution of model geometry (left), total shear strain (middle) and incremental shear strain (right) at (a) 250, (b) 500, (c) 750 and (d) 1000 m basement fault displacement for an experiment with thin salt layer and a basement fault dip of 70° without growth strata.

3.1.2. 60° dip fault

3.1.2.1. Experiment 3 - thick salt

From a first glimpse, the difference between the 60° and 70° dip fault is obvious. The geometry and total shear strain (Fig. 12a) show that after 250 m of displacement of the basement master fault a forced fold has developed in the cover sediments with a normal fault (M) propagating all the way from the edge of the salt layer to the top of the cover. This normal fault is cut on the top of the cover sediments by a steep reverse fault formed at the same time. Total shear strain spreads immediately above the basement fault tip and diffuses over the thick salt leading to a fanlike shape through the salt layer. The total shear strain shows a complex zone of steep and curved faults developing at the upper edge of the salt and propagating upwards, curving into the hanging-wall. The incremental shear strain shows that most of the deformation is accommodated by the salt at this stage.

At 500 m with continued displacement, two distinct groups of faults have developed (Fig. 12b). A group consists of two reverse faults formed in the hanging-wall while another group of two normal faults is developing further towards the footwall to the left of the previous normal fault (M). Total shear strain shows an increase and widening of the first zone of faulting that includes the normal fault (M) in addition to the other developing faults, while the incremental shear strain exhibits the continuing ability of salt to accommodate deformation due to the overall extension.

The next increments of displacement (750 and 1000 m total) show increasing displacement in the secondary faults, which become well defined both in the footwall and the hanging-wall (Fig. 12c, d). The total shear strain shows more deformation in the previous fault groups with evidences for more secondary faults yet to develop, while the incremental shear strain presents rapid weakening in the salt and hanging-wall faults with more deformation in the footwall.

The salt layer plays an important role in decoupling deformation between the formations below and above the salt layer. It can be seen how the salt flows by thinning in the footwall and thickening in the hanging wall. Furthermore, a collapse in the rightmost part of the model takes place as the displacement increases. Such collapse can be seen in other following models.

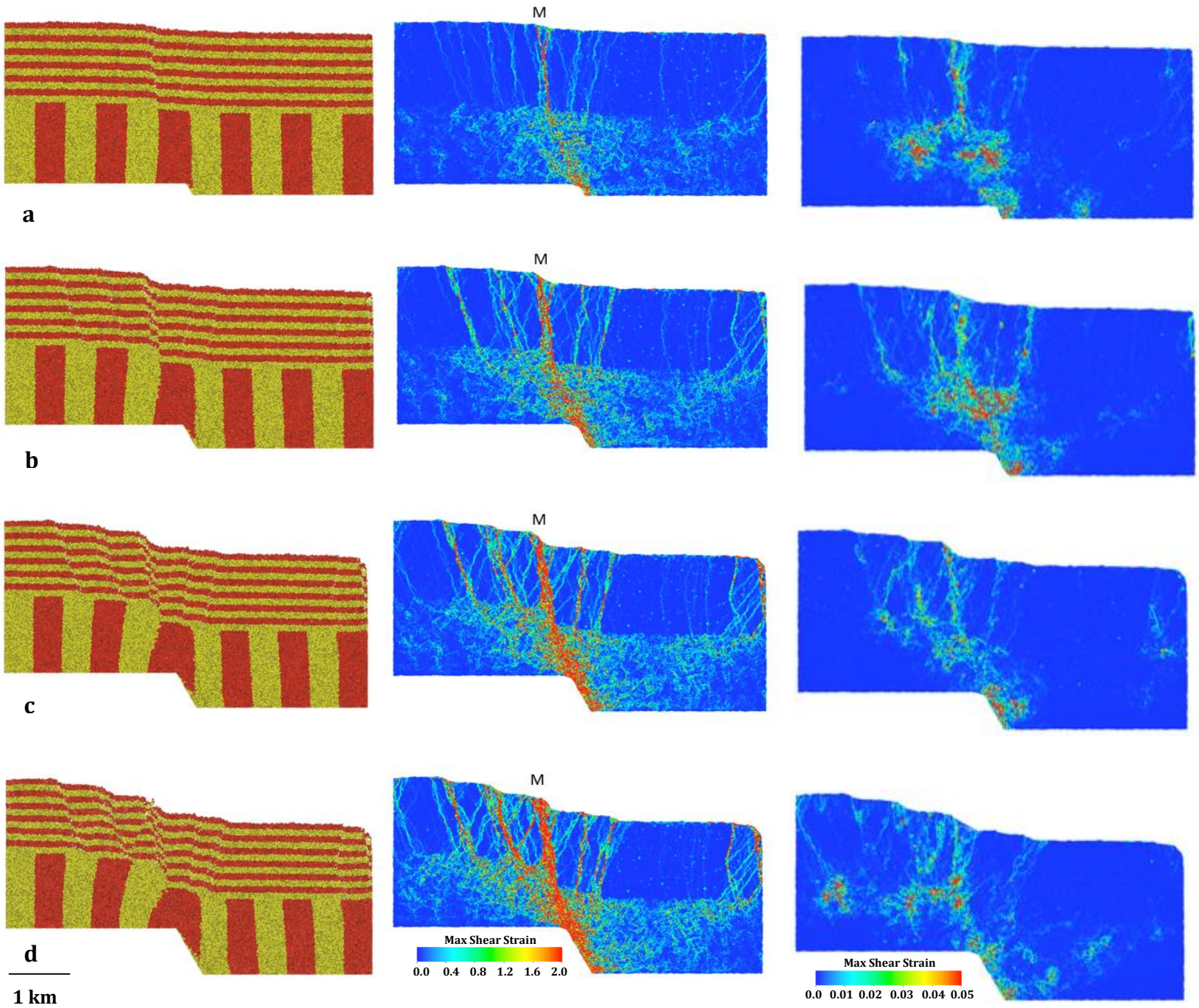

Figure 12. Evolution of model geometry (left) , total shear strain (middle) and incremental shear strain (right) at (a) 250, (b) 500, (c) 750 and (d) 1000 m basement fault displacement for an experiment with thick salt layer and a basement fault dip of 60° without growth strata.

3.1.2.2. Experiment 4 - thin salt

From the geometry and total shear strain (Fig. 13a), a forced fold can be observed clearly after 250 m of displacement of the basement master fault. A normal fault (M) and a curved reverse fault (R) develop simultaneously above the thin salt layer. Subsequently another normal fault (N) appears with similar dip angle to (M) located in the left to the previous normal fault further towards the footwall. The faults develop above the basement fault tip immediately over the thin salt layer in a narrow zone compared to the previous model. The total shear strain shows the structural style in the cover sediment as a zone of steep and curved faults, which have developed at the upper edge of the salt and propagate upwards. The incremental shear strain shows that deformation is strongly active on the normal fault (M) through the salt.

At 500 m with continued displacement, the incremental shear strain shows that the reverse fault (R) becomes essentially inactive with no increase in displacement, while the total shear strain expresses that normal faults are dominant with a notable increase in the faulting zone in between (Fig. 13b). Moreover, from the geometry and total shear strain it can be seen that two normal faults are under development in the footwall further to the left from the previous ones.

The following increments of displacement (750 and 1000m) display the increase in displacement and deformation in the secondary normal faults (Fig. 13c, d). The faulting zone becomes more complicated as the two normal faults (M, N) are trying to merge together along with new normal faults taking place in the footwall block further to the left, which can be seen clearly from the total shear strain. The incremental shear strain exhibits deformation activity in the normal faults further towards the footwall side. However, the whole setting is now divided into a well-defined hanging-wall and footwall.

From the initial stages of the model, the salt has showed slight influence in separating deformation between the sub-and supra-salt layers and this becomes more evident as the model advances. Also, it is clear that the normal faults in the footwall block of the cover sediments are approaching the dipping angle of the master normal fault as its displacement increases.

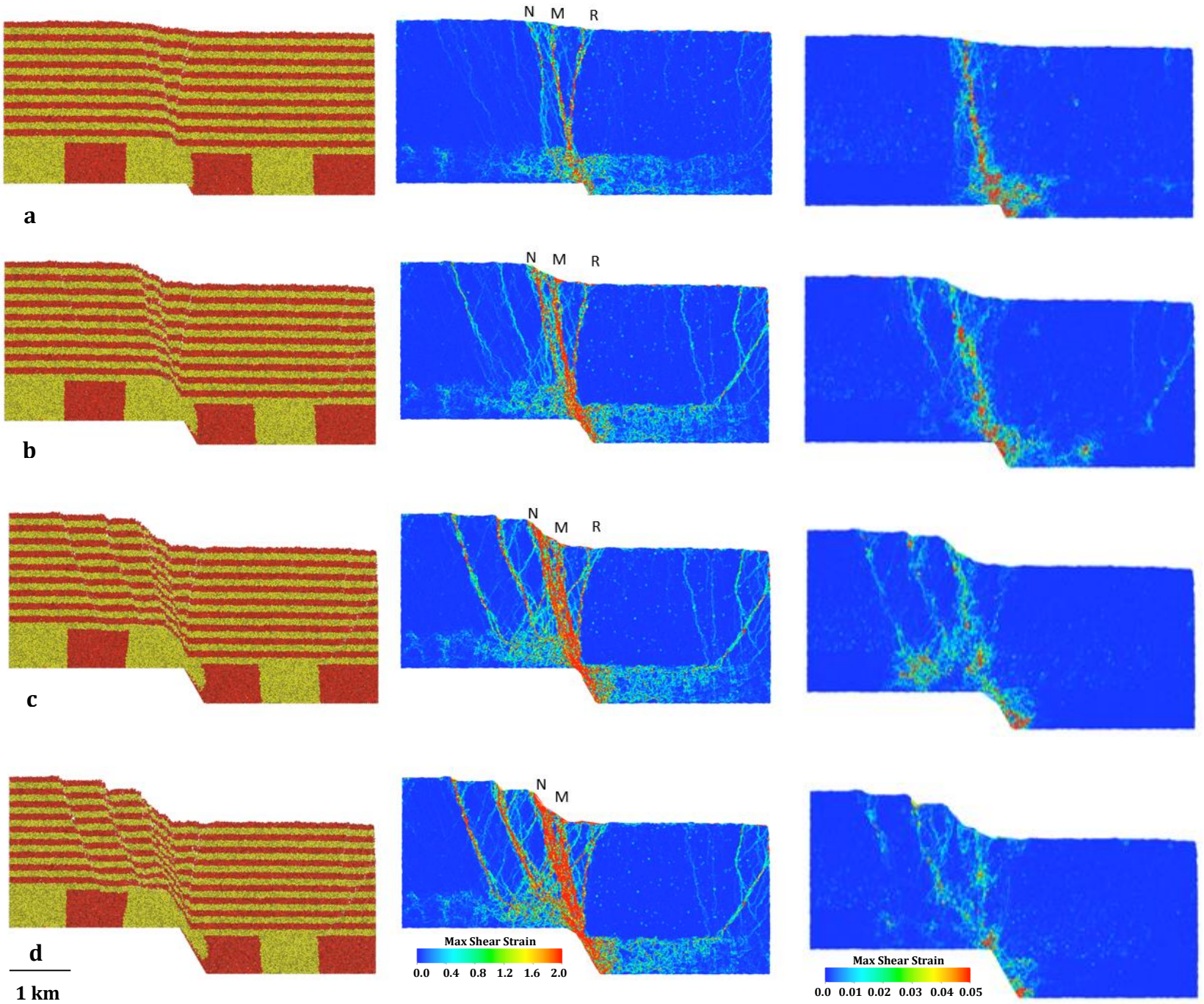

Figure 13. Evolution of model geometry (left) , total shear strain (middle) and incremental shear strain (right) at (a) 250, (b) 500, (c) 750 and (d) 1000 m basement fault displacement for an experiment with thin salt layer and a basement fault dip of 60° without growth strata.

3.1.3. 50° dip fault

3.1.3.1. Experiment 5 - thick salt

In all previous models, a reverse fault appears at the beginning of the simulation, followed or simultaneously with normal faults. With a 50° dipping master fault we can see the opposite. From the geometry and total shear strain (Fig. 14a), it can be observed that after 250 m of displacement a single normal fault (M) appears in the footwall side of the cover sediment. Shear strain spreads immediately above the basement fault tip and diffuses over the thick layer of salt leading to a fanlike shape throughout the salt layer. The total shear strain shows a development of several steep and curved faults both in the footwall and hanging-wall. The incremental shear strain shows some activity as a collapse or failure takes place in the rightmost part of the model.

At 500 m with continued displacement, two distinct groups of faults have developed widely through the cover sediments (Fig. 14b). The first one includes two reverse faults, which have developed in the hanging-wall, while the other one consists of two normal faults in the footwall where the previous fault (M) is centered between them. Total shear strain presents the developing faults over the cover sediments, while the incremental shear strain shows more activity for the salt in accommodating deformation further towards the footwall.

The later increments of displacement (750 and 1000 m total) express the increase in displacement in the secondary faults, which become well defined both in the footwall and hanging-wall (Fig. 14c, d). However, the faulting zone becomes more complex, most of the previous faults show evidence of splitting into one or more minor faults and more normal faults have developed in the last stages of extension. The complexity of the faulting zone in the footwall can be seen from the total shear strain while the incremental shear strain shows active deformation in the footwall along with attenuation of deformation in the hanging-wall.

On the other hand, the salt layer shows a significant influence in decoupling the deformation between the formations underneath and above the salt layer. Moreover, it can be noticed clearly how the salt flows by thinning in the footwall and thickening towards the hanging-wall.

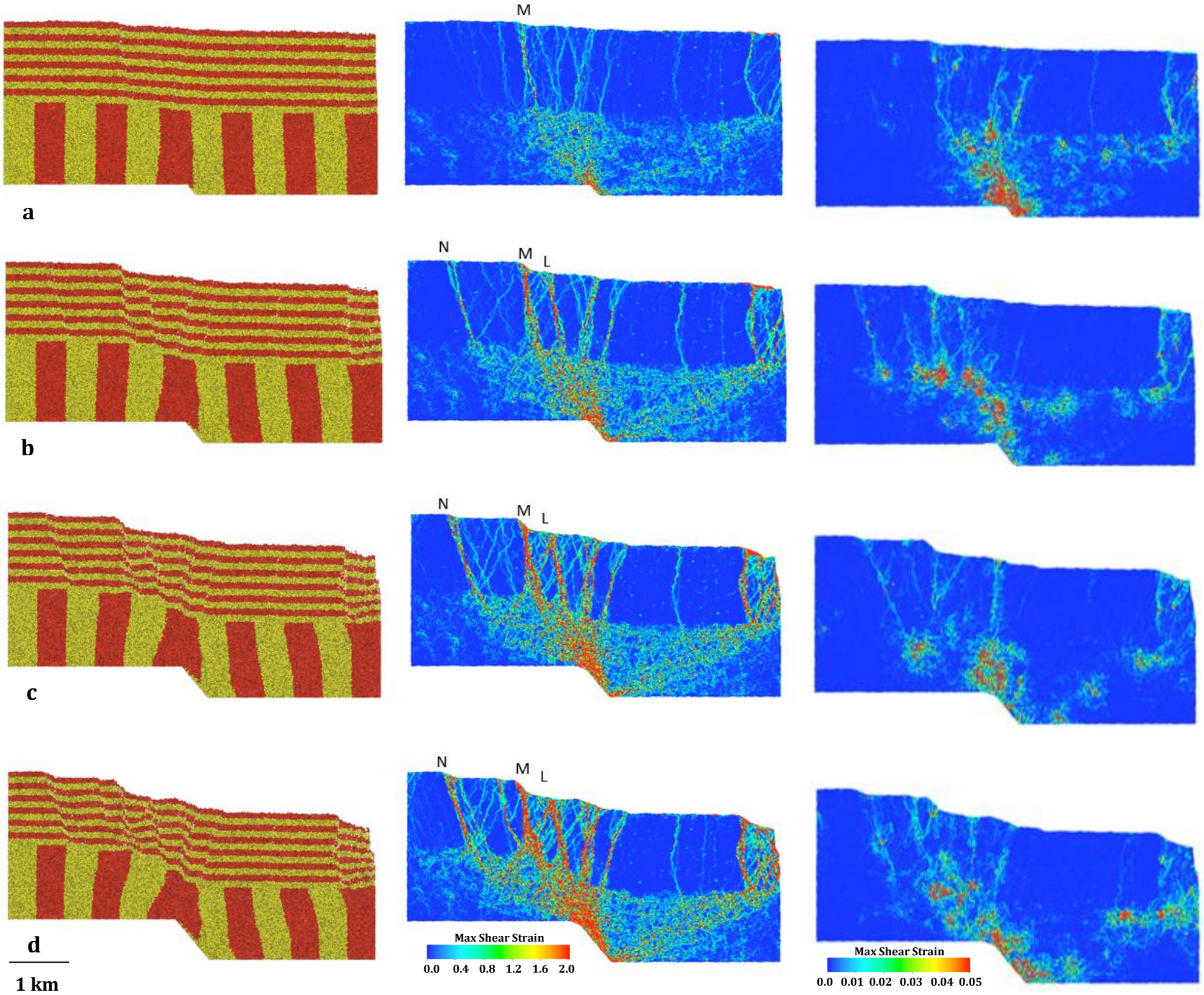

Figure 14. Evolution of model geometry (left), total shear strain (middle) and incremental shear strain (right) at (a) 250, (b) 500, (c) 750 and (d) 1000 m basement fault displacement for an experiment with thick salt layer and a basement fault dip of 50° without growth strata.

3.1.3.2. Experiment 6 - thin salt

Similarly to the previous model, no reverse fault can be noticed in the first stages of deformation. The difference this time is that at 250 m of fault displacement, two normal faults have developed in the footwall and clearly can be observed from the geometry and total shear strain (Fig. 15a). However, one of them (M) develops directly above the basement fault tip over the thin salt layer, while the other one (N) is located just to the left of the pervious with less displacement magnitude. The normal fault (M) curves partially towards the hanging-wall at the top of the cover sediment forming a small minor reverse fault. The total shear strain shows the zone of steep and curved faults, which developed at the upper edge of the salt and have propagated upwards while the incremental shear strain exhibits that most deformation is in the salt and the fault (M).

At 500 m with continued displacement (Fig. 15b), the normal faults are more dominant with a notable increase in the faulting zone with more faulting as the displacement increase. The incremental shear strain shows that the deformation in this stage turns towards the fault (N) while there is no activity in (M). Furthermore, total shear strain shows that another normal faults are under development in the footwall further to the left from the former.

In the following increments of displacement (750 and 1000m) the faulting zone becomes more complex with new normal faults in the footwall side of the cover sediments (Fig. 15c, d). The normal fault (N) as well as the new faults in the footwall approach the dipping angle of the master fault, while the activity of fault (M) is highly decreasing as can be noticed from the incremental shear strain. The incremental shear strain also shows some active deformation in the hanging-wall as well as the footwall. However, the whole setting is now divided into a well-defined hanging-wall and footwall.

For this model, no reverse faults formed during the entire process of simulation. The thin salt layer shows no significant impact in decoupling the deformation between the sub- and supra-salt layers.

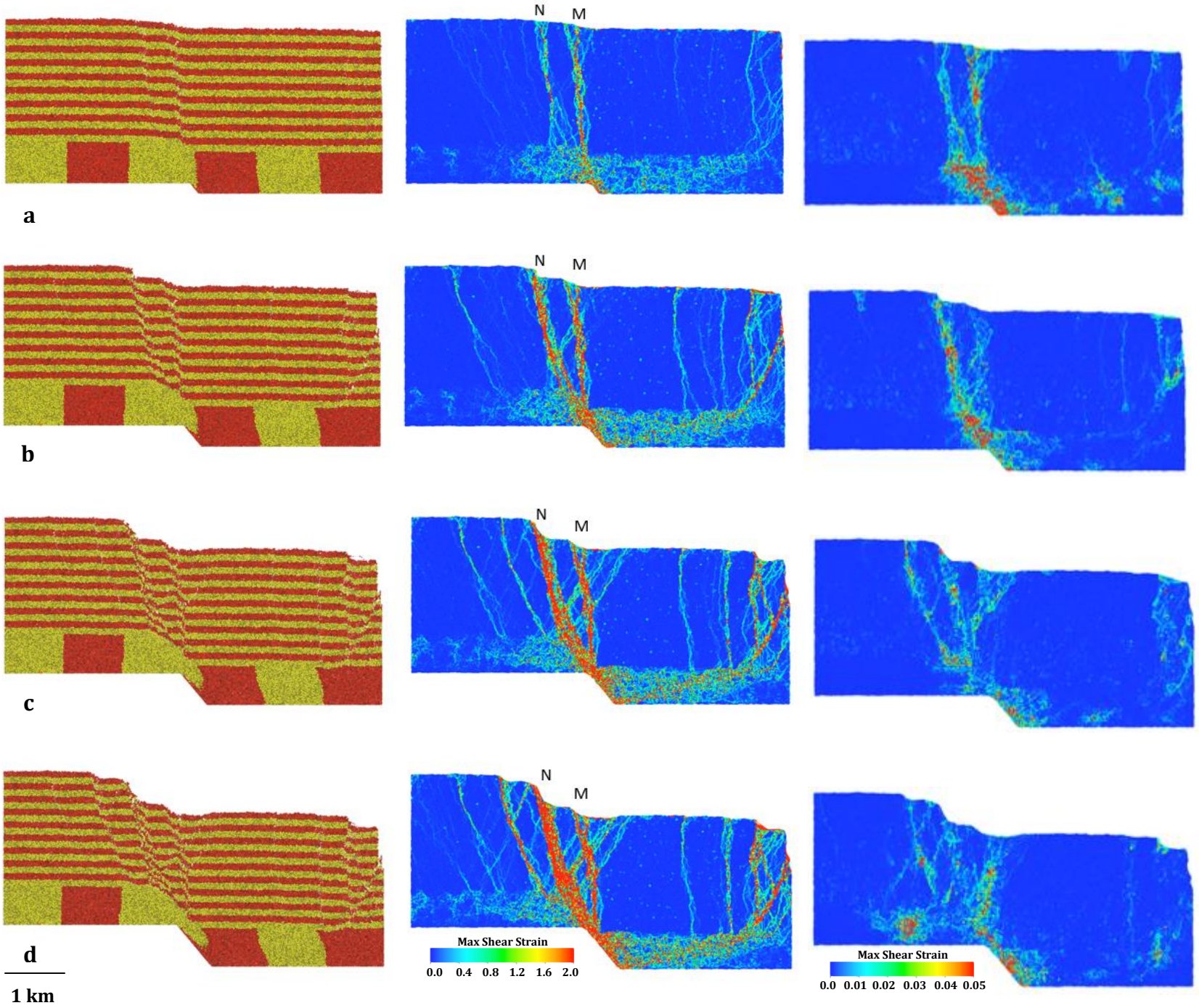

Figure 15. Evolution of model geometry (left), total shear strain (middle) and incremental shear strain (right) at (a) 250, (b) 500, (c) 750 and (d) 1000 m basement fault displacement for an experiment with thin salt layer and a basement fault dip of 70° without growth strata.

3.2. Models with growth strata

3.2.1. 70° dip fault

3.2.1.1. Experiment 7 - thick salt

From the geometry and total shear strain (Fig. 16a), it can be observed that after 250 m displacement of the basement master fault a forced fold has developed in the cover sediments with a notable steep set of faults. The shear strain spreads immediately above the basement fault tip and diffuses over the thick layer of salt leading to a fanlike shape over the salt layer. A steep reverse fault (R) has developed in the hanging-wall and splits at the top into two small branches. Almost three steep normal faults (M, N and L) can be observed in the footwall. These faults are still under development and can be observed only from the total shear strain. The incremental shear strain shows that most of the deformation takes place in the salt in addition to the faults (M and N).

At 500 m with continued displacement and increasing sedimentation, the faulting zone has increased between the two normal faults (M, N) while a new fault has developed further to the left of the previous ones (Fig. 16b). On the other hand, the incremental shear strain shows no active deformation on the reverse fault (R).

For the next increments of displacement (750 and 1000 m total) the fault zone becomes wider in the footwall with some linkage between (M and N) in addition to a new normal fault developing to the left of the previous ones (Fig. 16c, d). The previous fault (R) is partly inactive with negligible deformation as can be seen from the incremental shear strain while active deformation is happening at the central faults (M, N), which almost become one fault. The total shear strain shows more deformation in the previous faulting zones in the footwall with evidence for more secondary faults yet to develop.

At this stage, it can be noticed how the salt is effective in decoupling the sub- and supra-salt layers as the master fault does not propagate all the way upwards; instead, different type of deformation has formed in the cover sediments. It can be noticed how the salt above basement flows by thinning above the footwall and thickening above the hanging-wall.

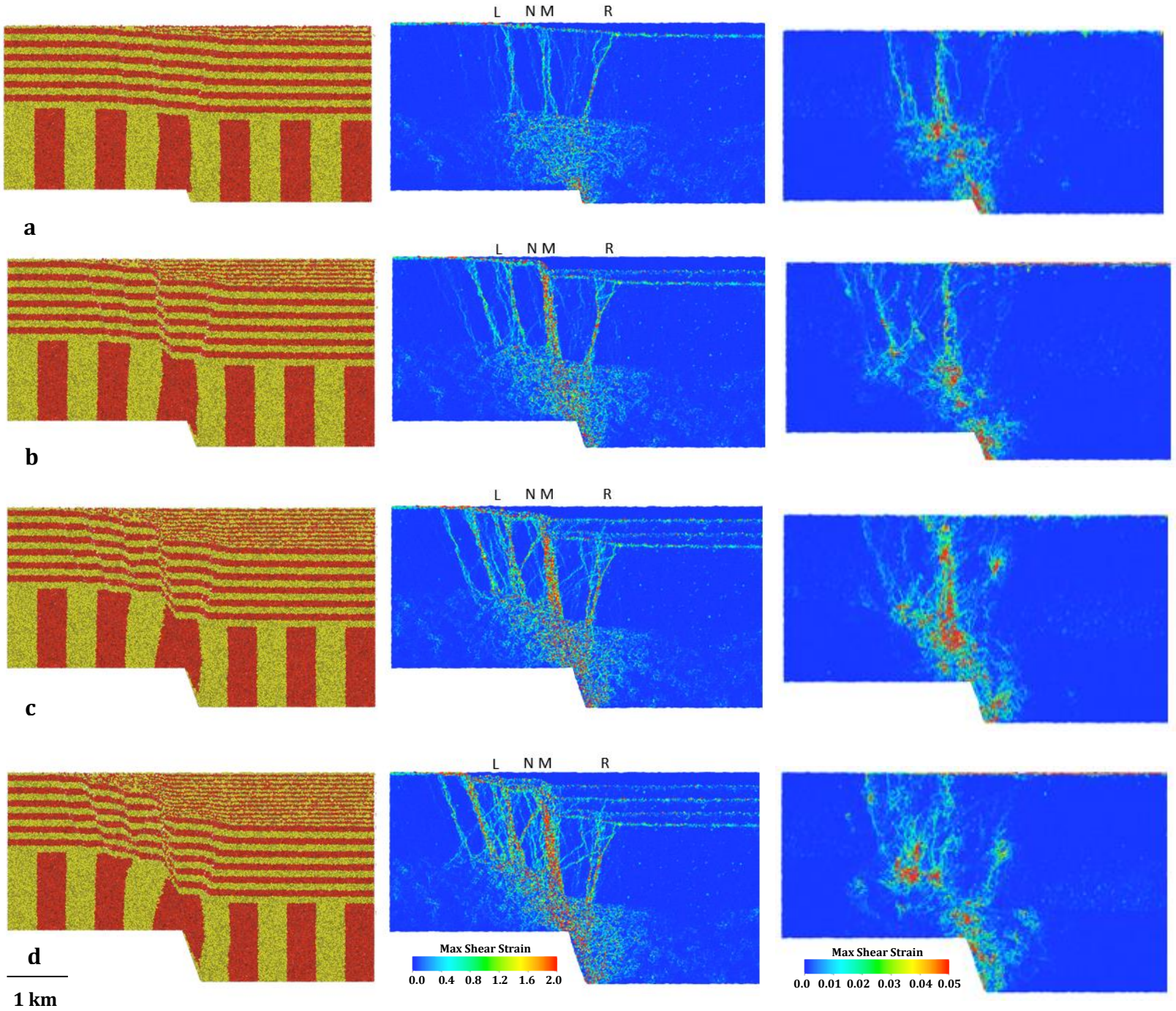

Figure 16. Evolution of model geometry (left), total shear strain (middle) and incremental shear strain (right) at (a) 250, (b) 500, (c) 750 and (d) 1000 m basement fault displacement for an experiment with thick salt layer and a basement fault dip of 70° with growth sediments.

3.2.1.2. Experiment 8 - thin salt

For the first increment of displacement (250 m) the forced fold can be observed within a relatively narrow zone of faulting in the cover sediments. A steep reverse fault (R) has developed first in the hanging-wall, subsequently followed by a normal fault (M) in the footwall (Fig. 17a). The reverse fault (R) forms at the top of the salt layer with a significant displacement and diminishing gradually until disappear at the top of the cover sediments. In contrast, the normal fault (M) has its largest displacement in the middle of the cover and weakens towards the salt layer. The total shear strain shows the zone of steep faults, which develops at the upper edge of the salt and propagates upwards as well as other secondary faults yet under development, while most of the deformation is accommodated by the salt as can be seen from the incremental shear strain.

At (500 m) with continued displacement and increased sedimentation, the total shear strain shows that the reverse fault splits into several minor and curved faults with a notable increase in the faulting zone in between of them while from the incremental shear strain, the change from reverse to normal fault could be seen clearly (Fig. 17b). Moreover, the normal fault zone becomes slightly wider with a major increase in displacement.

In the following increments of displacement (750 and 1000m), the deformation becomes more complicated in which most of the faults cannot be traced clearly (Fig. 17c, d). The incremental shear strain shows decrease of deformation in the hanging-wall of the cover sediments along with more activity towards the footwall structures. In the last stage of displacement, a new curved normal fault has developed further to the left of the fault (M) in the footwall side. However, the whole setting now is divided into a well-defined hanging wall and footwall.

On the other hand, the thin salt layer shows no significant impact in decoupling the deformation between the sub- and supra-salt layers. It can be noticed that the normal fault (M) has almost similar dip angle as the master normal fault.

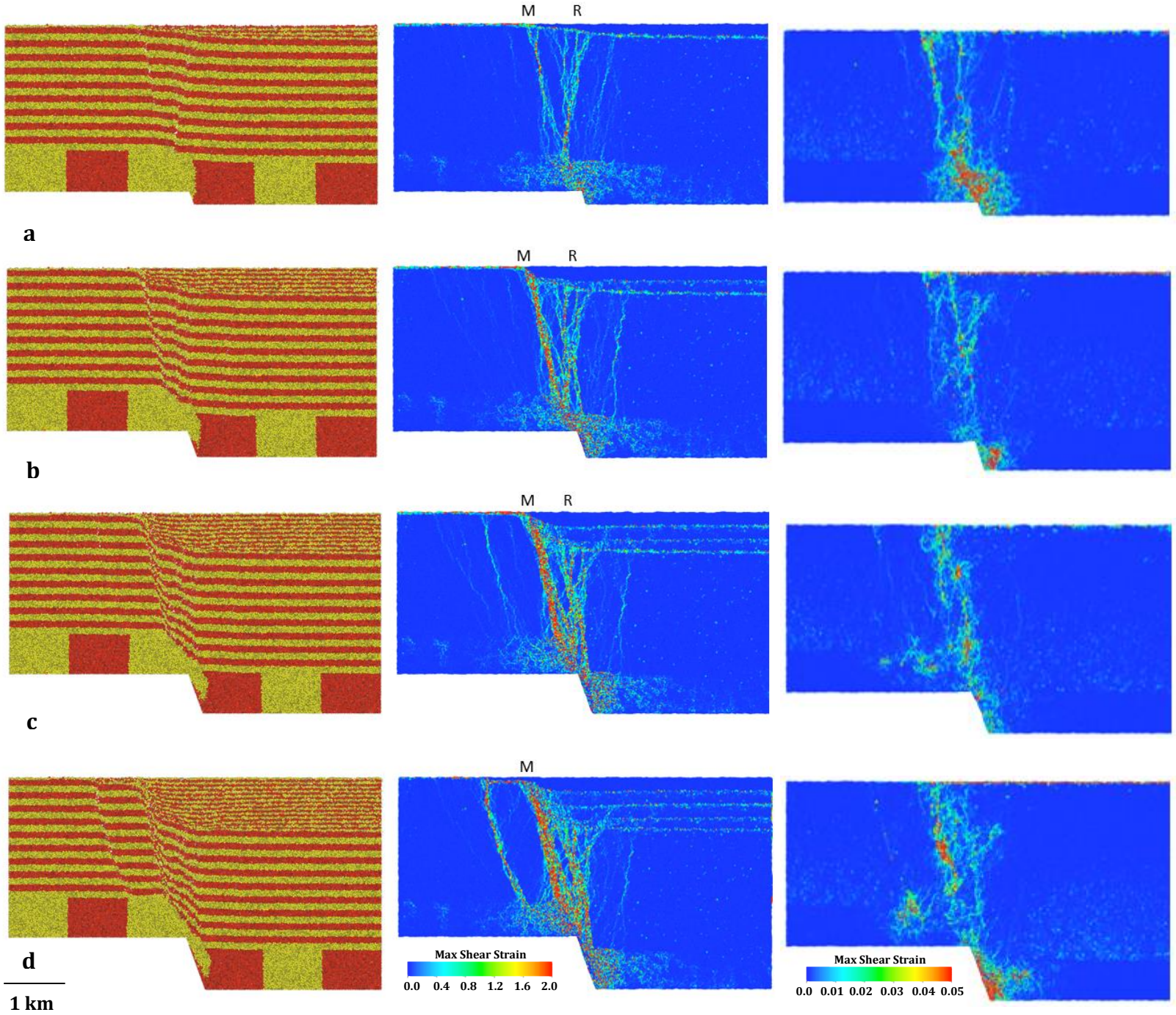

Figure 17. Evolution of model geometry (left), total shear strain (middle) and incremental shear strain (right) at (a) 250, (b) 500, (c) 750 and (d) 1000 m basement fault displacement for an experiment with thin salt layer and a basement fault dip of 70° with growth sediments.

3.2.2. 60° dip fault

3.2.2.1. Experiment 9 - thick salt

In this experiment after 250 m of displacement of the basement master fault, a different set of faults develops in the sedimentary cover (Fig. 18a). At the beginning of the simulation, a very steep reverse fault (R) forms above the thick salt layer. This fault is hardly recognized at the base of the cover sediments but further upward the steep reverse fault could be clearly defined. However, this fault shows some curving in the middle of the cover towards the hanging-wall. Subsequently a normal fault (M) has just developed in the footwall side and again it has a clear offset at the top half but it is difficult to trace at the bottom half of the cover sediment. Total shear strain spreads immediately above the basement fault tip and diffuses over the thick layer of salt leading to a fanlike shape through the salt layer, while the incremental shear strain shows that most of the deformation takes place in the salt.

At 500 m with continued displacement and increasing sedimentation, the faulting zone has increased and more faults have formed both in the hanging wall and footwall (Fig. 18b). The previous reverse fault (R) has turned into two related normal faults clearly observed at the top of the cover sediments, while it is hardly defined at the bottom. In addition, two new curved faults have developed; a reverse fault in the hanging-wall and a normal fault in the footwall. The salt still accommodates most of the deformation as can be seen from the incremental shear strain.

The next increments of displacement (750 and 1000 m total) express the complexity of the former faulting zone while no new faults has formed (Fig. 18c, d). The total shear strain shows more deformation through the previous faults with evidences for more secondary faults yet to develop, while the incremental shear strain shows less deformation in the hanging-wall side along with increasing activity in the footwall.

At this stage, it can be noticed how the salt is being effective in decoupling the sub- and supra-salt layers as the master fault does not propagate all the way upwards. Also, different types of deformation have formed in the cover sediments due to the salt effect. Furthermore, it can be noticed how the salt above the basement flows by thinning above the footwall and thickening above the hanging-wall.

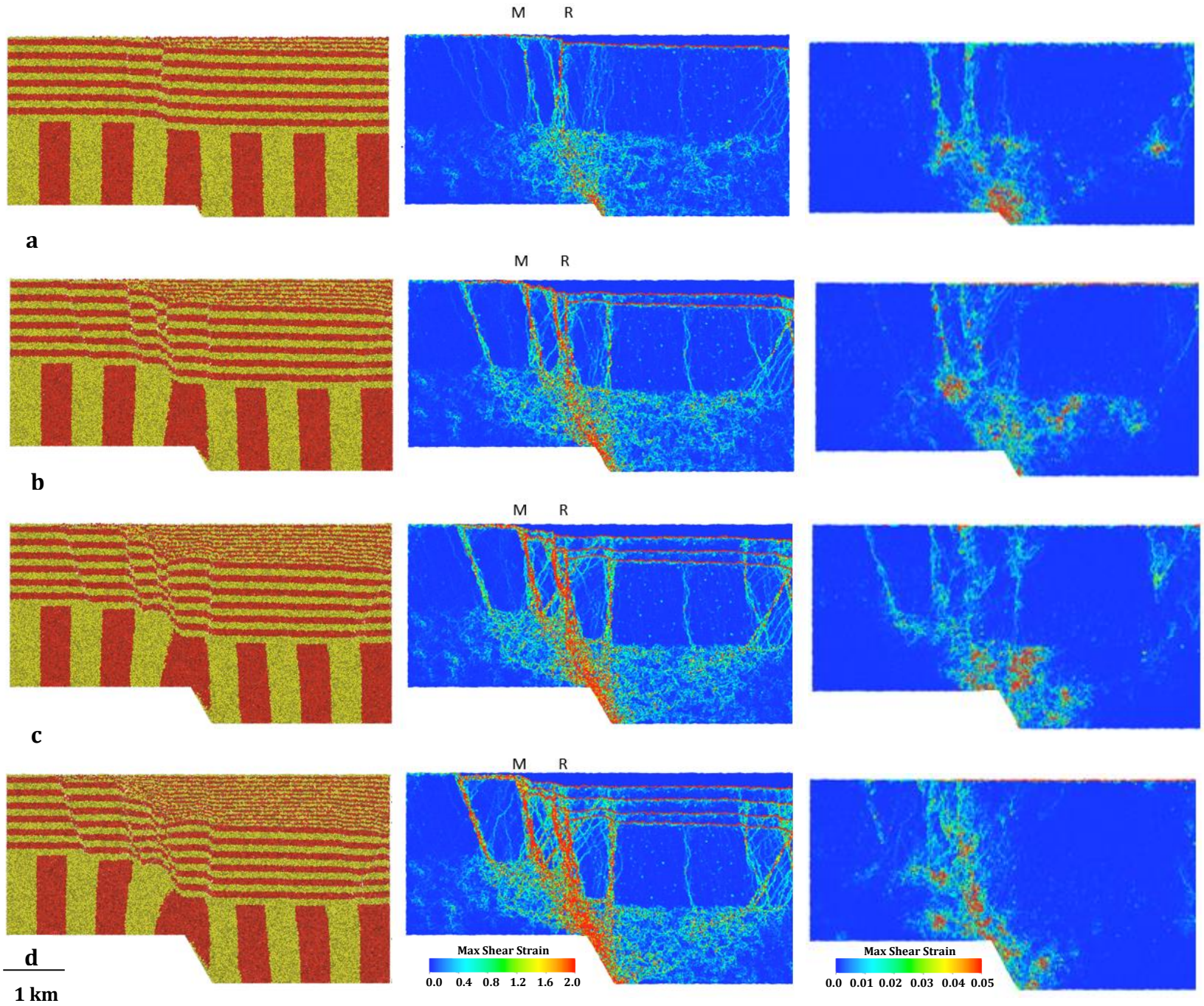

Figure 18. Evolution of model geometry (left), total shear strain (middle) and incremental shear strain (right) at (a) 250, (b) 500, (c) 750 and (d) 1000 m basement fault displacement for an experiment with thick salt layer and a basement fault dip of 60° with growth sediments.

3.2.2.2. Experiment 10 - thin salt

For the first increment of displacement at 250 m the forced fold can be observed within a relatively narrow zone of faulting in the cover sediments (Fig. 19a). This time a single normal fault (M) has developed first at the edge of the salt layer and then propagates upward with some fracturing in the middle of the cover sediment. The total and incremental shear strains spread immediately above the basement fault tip and diffuse in a narrow zone over the thin layer of salt leading to a small fanlike shape through the salt layer.

At 500 m with continued displacement and increase sedimentation, the result becomes a bit complex (Fig. 19b). More deformation is taking place on the former normal fault, which leads to increase in the width of the fault zone. Moreover, a zone of faulting (R) has developed in the hanging-wall at the edge of salt with a short reverse fault curving rapidly until switches into a normal fault, which itself subsequently turns into two normal faults diminishing gradually towards the top of the cover sediments. The total shear strain exhibits this complexity in deformation while the incremental shear strain shows that most of the deformation takes place in the fault (M) at this increment.

In the following increments of displacement (750 and 1000m) the deformation becomes more complicated and the previous faults are not well-defined separately (Fig. 19c, d). Total and incremental shear strains show that a curved normal fault (N) has formed further to the left of the previous one in the footwall side while another one is under development in the last stage of displacement. The whole setting is now divided into a well-defined hanging wall and footwall. On the other hand, the thin salt layer shows no significant impact in decoupling the deformation between the sub- and supra-salt layers.

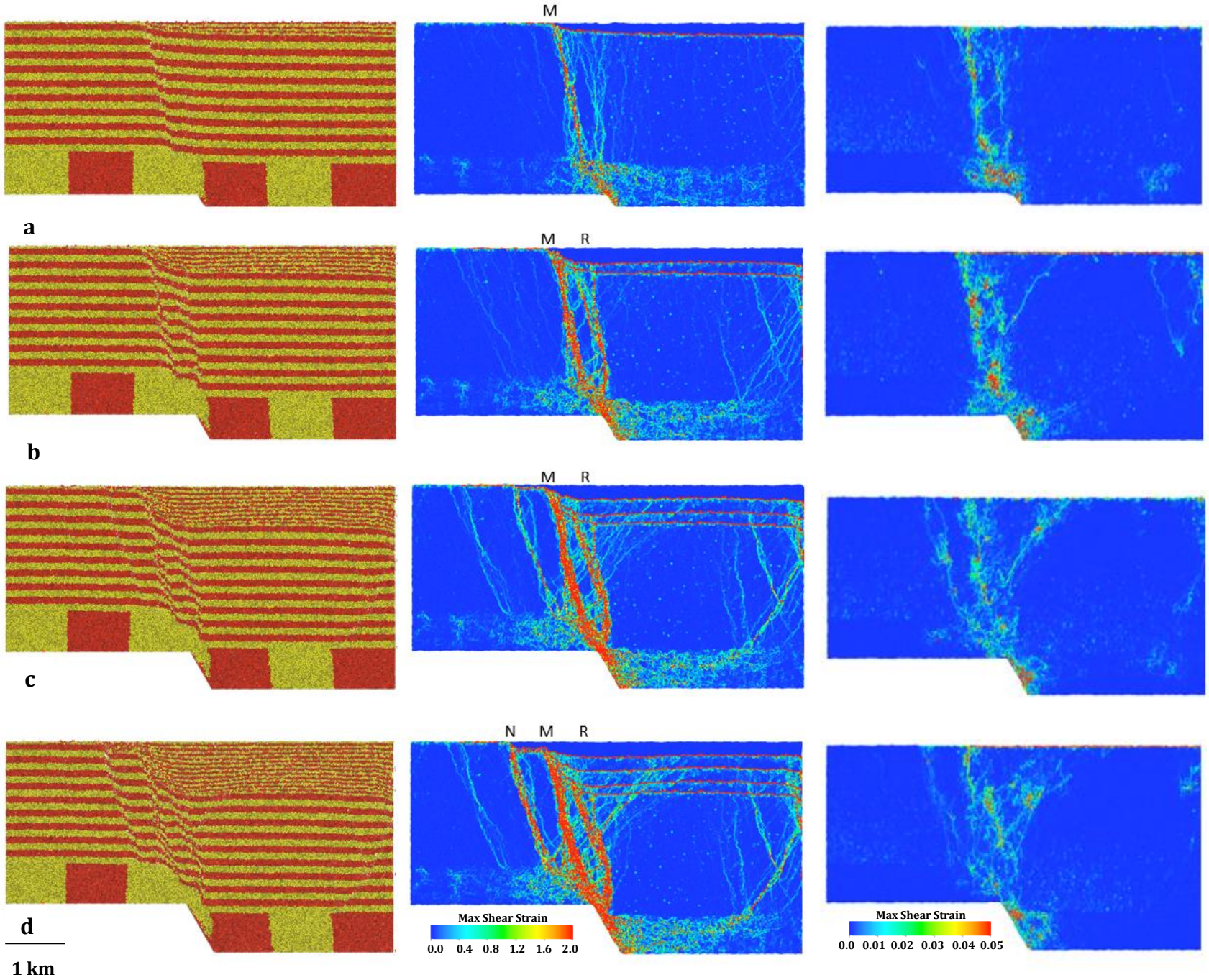

Figure 19. Evolution of model geometry (left), total shear strain (middle) and incremental shear strain (right) at (a) 250, (b) 500, (c) 750 and (d) 1000 m basement fault displacement for an experiment with thin salt layer and a basement fault dip of 60° with growth sediments.

3.2.3. 50° dip fault

3.2.3.1. Experiment 11 - thick salt

From the geometry and total shear strain (Fig. 20a), it can be observed that after 250 m of displacement of the basement master normal fault a monocline develops in the cover sediments with notable three steep faults. A steep reverse fault (R) has developed in the hanging-wall and splits at the top into two small branches. It has remarkable displacement at the lower half of the cover sediments while decreasing in displacement upwards. Almost two steep normal faults still in development (M, N) can be observed in the footwall as well. The fault (M) can be defined well from both the geometry and shear strain while (N) appears in the total shear strain as a curved fault changing from normal to reverse as it propagates upwards with almost a negligible displacement. Total and incremental shear strains spread out immediately above the basement fault tip and diffuse over the thick layer of salt leading to a fanlike shape throughout the salt layer.

At 500 m with continued displacement and increasing sedimentation, the faulting zone has increased for the two normal faults (M, N) while a new fault is developing further to the left of the previous ones (Fig. 20b). The fault (N) can be well-defined as a normal fault while the reverse fault (R) has no activity as can be seen from the incremental shear strain.

For the next increments of displacement (750 and 1000 m total), the faulting zone becomes wider in the footwall with more faulting (Fig. 20c, d). The incremental shear strain expresses that no activity takes place anymore in the previous reverse fault (R). The total and incremental shear strains show more deformation in the previous faulting zones while more normal faults are developing in the footwall.

Furthermore, it can be noticed how the salt is effective in decoupling the sub- and supra-salt layers as the master fault does not propagate all the way upwards where different type of deformation has formed in the cover sediments. However, salt shows less influence in decoupling deformation with increasing displacement. Also it can be noticed how the salt above basement flows by thinning above the footwall and thickening above the hanging-wall.

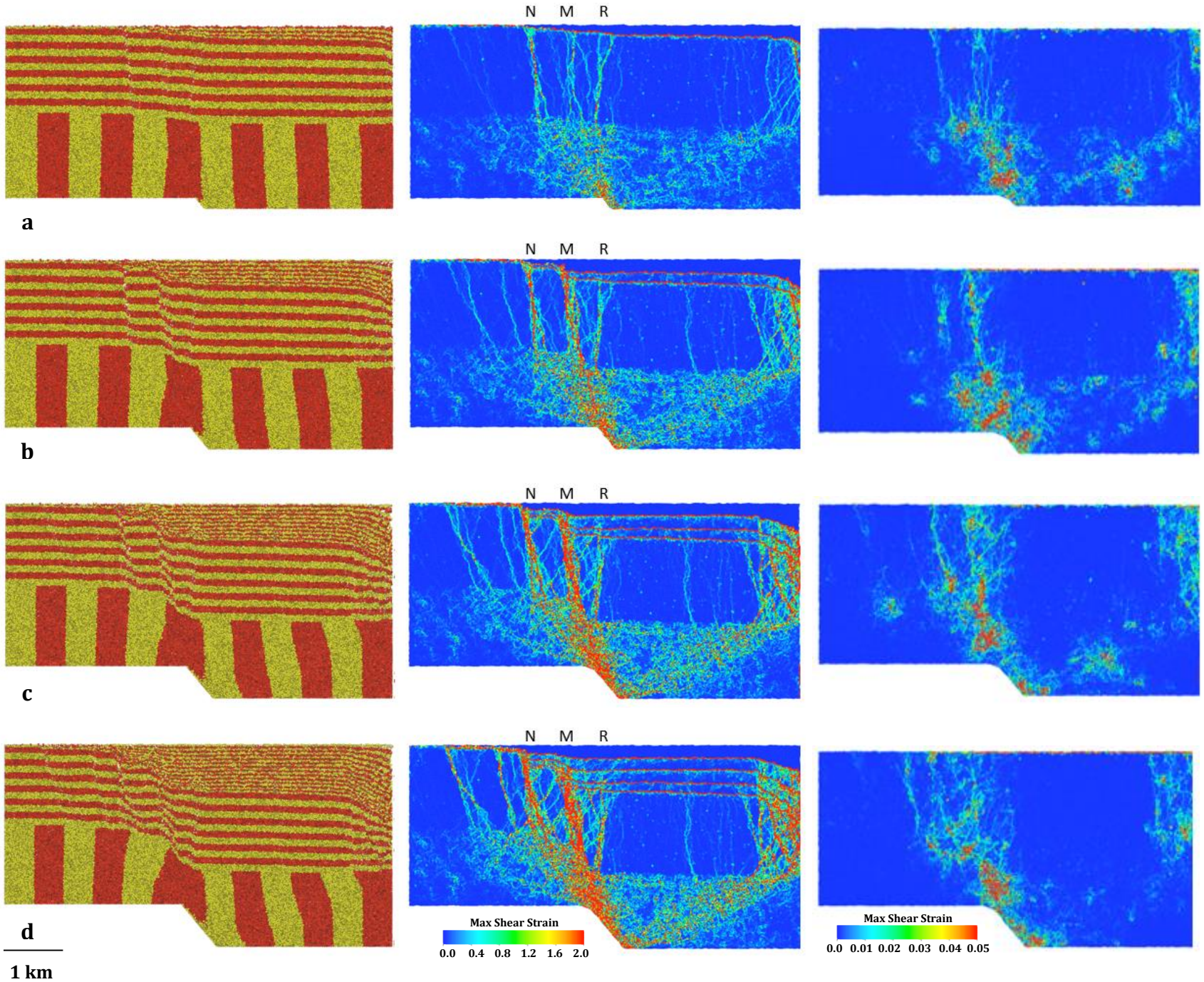

Figure 20. Evolution of model geometry (left), total shear strain (middle) and incremental shear strain (right) at (a) 250, (b) 500, (c) 750 and (d) 1000 m basement fault displacement for an experiment with thick salt layer and a basement fault dip of 50° with growth sediments.

3.2.3.2. Experiment 12 – thin salt

For the first increment of displacement at 250 m the forced fold can be observed within a relatively narrow zone of faulting in the cover sediments (Fig. 21a). At this stage, a single normal fault (M) has developed first at the edge of the thin salt layer and then propagates upward with some fracturing in the middle of the cover sediment. The total shear strain spreads immediately above the basement fault tip and diffuses in a narrow zone over the thin layer of salt leading to a fanlike shape through the salt layer. The incremental shear strain expresses the intensity of deformation taking place on the normal fault (M).

Contrary to the previous (60°) model in experiment (10), at 500 m of the model extension no new faults appears or form in the hanging-wall while more deformation takes place on the former normal fault (Fig. 21b). The complexity of faulting expressed by more faulting and widening of the fault zone can be seen from the total shear strain.

In the following increments of displacement (750 and 1000 m) the deformation becomes more complicated in comparison to the previous results (Fig. 21c, d). A new curved normal fault (N) has formed further to the left of the previous one in the footwall side and eventually separates into two branches at the top of the cover sediments. The incremental shear strain shows active deformation in the normal faults with more concentration on the fault (M). Another observation is that no reverse fault appears in the hanging-wall for the entire process of extension.

The whole setting is now divided into a well-defined hanging-wall and footwall. However, the thin salt layer shows no substantial influence in decoupling the deformation between the sub- and supra-salt strata.

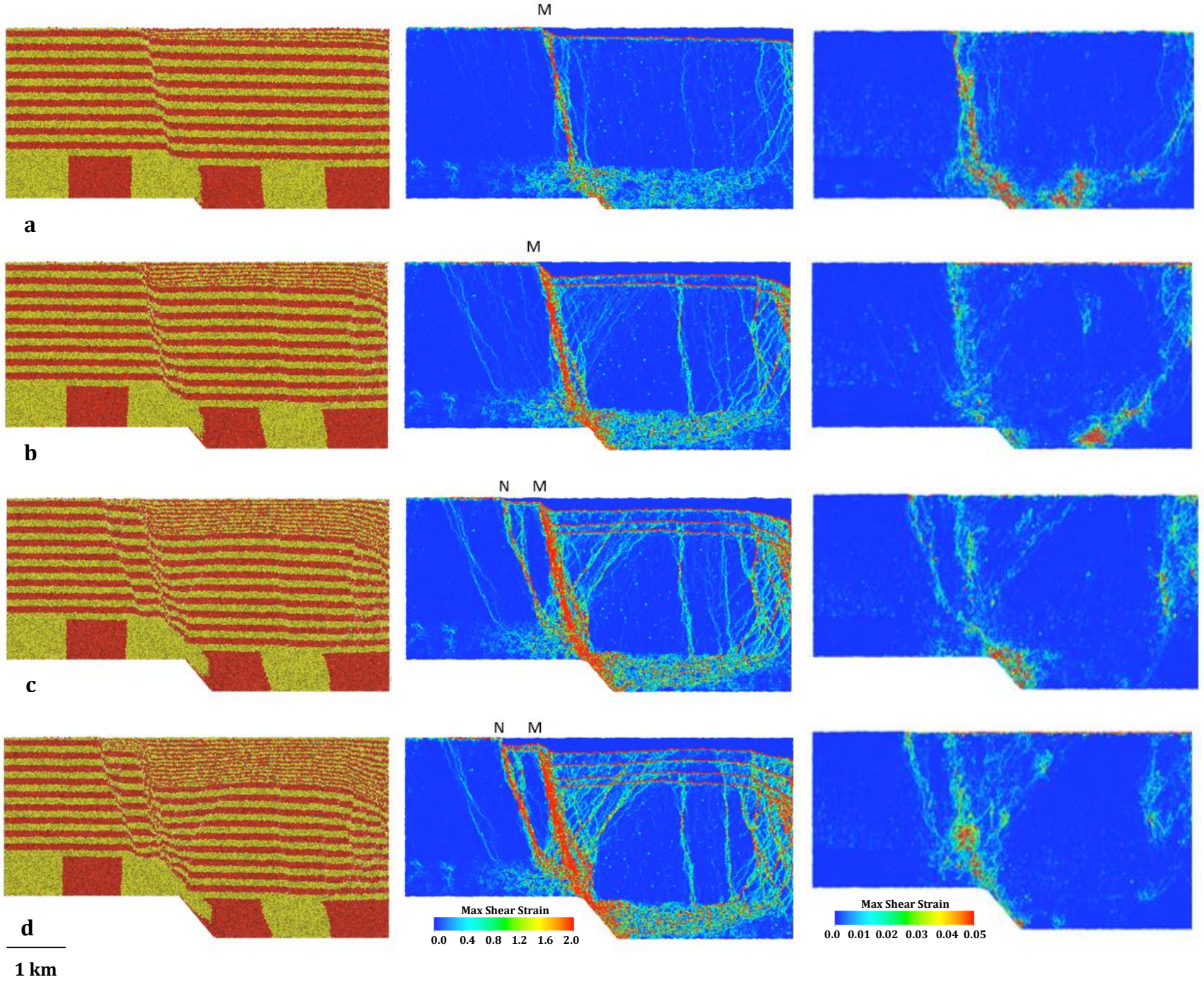

Figure 21. Evolution of model geometry (left), total shear strain (middle) and incremental shear strain (right) at (a) 250, (b) 500, (c) 750 and (d) 1000 m basement fault displacement for an experiment with thin salt layer and a basement fault dip of 50° with growth sediments.

4. Discussion and Conclusion

In this thesis, discrete element models are used to systematically study and examine the influence of a ductile salt layer on the deformation patterns and structural styles associated with basement-involved extensional forced folding. As outcome, these models suggest that the geometry of extensional forced folds and their related secondary structures are strongly influenced by the thickness of the salt layer. In addition, the basement fault dip angle also has a significant impact on the modeling results.

From the performed simulations, the impact of salt thickness in deformation styles in the cover sediment can be stated as follows: with a thick salt layer, deformation and resultant structural patterns in the cover sequence are widely distributed. In fact, a broad monocline develops above the salt layer as well as secondary reverse and normal faults within the cover sequence. The models suggest that the developing monocline width is directly proportional to the salt layer thickness.

For the models with thick salt layer, decoupling between the sub- and supra-salt layers is effective. In other words, the thick salt considerably decouples the deformation of the basement from the overburden. The decoupling between sub- and supra-salt deformations occurs due to the salt ductility and halokinesis. This takes place as the salt layer accommodates the slip along the basement fault by thinning above the footwall and thickening above the hanging wall. The thinning and thickening mechanism of the salt occurs by flow from the upthrown side – above the basement footwall – towards the downthrown side of the hanging-wall.

In contrast, models with a thin salt layer show no substantial influence of the salt in decoupling the deformation between the sub- and supra-salt strata. The results show that a thin salt layer spreads and diffuses deformation above a basement master fault directly over the cover sediments. According to (Vendeville et al., 1995), the deficiency of such thin salt layer to decouple deformations between sub- and supra-salt formations is because it has no ability to transmit differential stresses high enough to permit localized deformation in areas away from the master fault. However, still deformation in the cover strata takes place in the form of forced folding.

Normal and reverse faults are present in the simulations. In most of the results, reverse faults are the first structures to develop while in some experiments normal faults are the first to develop. The structural styles above the basement normal fault are asymmetric as the deformation initiates normally in the hanging-wall – in most cases - and migrates towards the footwall in the form of normal faults, forming a triangular shape over the cover sediments. In many models this migration of deformation takes place through the death of the earlier reverse faults developing in the hanging-wall followed by growth of normal faults in the footwall.

As the displacement on the master normal fault increases, the evaporite layer thins near the edge of the footwall block and a linkage between the secondary normal faults and the master normal fault begin to form through the salt due to the attenuation of the salt layer. Also, more secondary faults develop in the footwall of the cover sequence as the displacement on the basement master fault increases. Another point is that the dip angle of these secondary normal faults tends to increase as they develop far from the master normal fault in the footwall block.

Another aspect of the deformation mechanism for the forced fold is the temporal evolution of the secondary structures in the cover sediments. The results indicate that some of the secondary structures adjacent to the basement normal faults are not all active at the same time as they might form and die at different stages during the model evolution.

The dip angle as well has an influence on the resultant structural styles. However, in the presence of a thick salt layer, there are no large variations in deformations related to different master fault dip angles. The main manifestation of such models involves wide faulted forced folds with more secondary structures in the footwall of the cover sediments. The difference between these models exists in the geometry evolution of each one as they differ normally in the first stages of the extension. While in some models reverse fault is the first secondary fault to develop, in others the deformation initiates by normal faulting in the cover strata.

Moreover, in models with a thin salt layer the resultant structures vary slightly as the dip angle of the master fault changes. A narrow zone of deformation represents these models at the early stages of modeling. However, this changes as the displacement in the master fault increases in the models with 60° and 50° dip angle as more secondary normal

faults develop in the footwall side. One more observation is that for the 50° master fault, no reverse fault exists from the beginning till the end of the extension. Although the curved shape of the secondary faults is a dominant concept in most of such models, it is highly exposed and more obvious with the 50° master fault dip angle.

The growth sedimentation also influences the deformation style and the mechanical geometry of most of the models. In all models with growth strata, the geometry evolution is slower in comparison with those without. However, this is demonstrated by less secondary faults in the footwall and specifically with notable decrease in deformation in the hanging-wall of the cover sediments. Overall, the structural styles between models with growth strata and their corresponding without growth strata remain similar to far extent as both are characterized by wide faulted monoclines with thick salt, while they become narrower where the salt is thin. However, the growth beds are also folded along with the cover sediments, thinning toward the footwall of the master normal fault while dipping and thickening in the hanging-wall block.

In fact, in many extensional systems with salt such as those in the North Sea, offshore Norway and the Gulf of Suez (Khalil and McClay, 2002; Sharp et al., 2000), hydrocarbons are normally trapped within the secondary structures associated with extensional forced folding. The outcomes of this study modeling can provide some useful guidelines for recognizing and defining the structural traps within the supra-salt deformation settings. For example and as described previously, a monocline within the cover sediment above the salt is produced due to the displacement on the basement normal fault. The monocline's width varies substantially depending on several factors and the thickness of the salt is a major one. As a result numerous secondary and minor normal and reverse faults form and possibly cut and weaken the developed monocline or forced fold. In addition, growth strata related to the extensional forced folding dip and thicken in the hanging-wall block of the cover sequence away from the master normal fault. Such observations might be valuable and have substantial implications on the exploration and development of oil and gas prospects.

Fault zones and their related systems have a significant role in the development and control of the mechanical and fluid flow properties of the Earth crust, besides the architecture of sedimentary deposits (Faulkner et al., 2010). Although real faults are three-

dimensional structures and undoubtedly 3D modeling would be much convenient, the 2D models in this study give helpful insights on the mechanical behavior of basement-involved salt influenced extensional forced folding.

References

Allen, M. P., and Tildesley, D. J., 1987, Computer simulation of liquids, Clarendon Press.

Bagi, K., 2006, Analysis of microstructural strain tensors for granular assemblies: International Journal of Solids and Structures, v. 43, no. 10, p. 3166-3184.

Bathe, K. J., 1996, Finite Element Procedures, Prentice Hall.

Botter, C., Cardozo, N., Hardy, S., Lecomte, I., and Escalona, A., 2014, From mechanical modeling to seismic imaging of faults: A synthetic workflow to study the impact of faults on seismic: Marine and Petroleum Geology, v. 57, p. 187-207.

Cardozo, N., and Allmendinger, R. W., 2009, SSPX: A program to compute strain from displacement/velocity data: Computers & Geosciences, v. 35, no. 6, p. 1343-1357.

Cosgrove, J. W., 1999, Forced folds and fractures: An introduction: Geological Society, London, Special Publications, v. 169, no. 1, p. 1-6.

Cundall, P. A., 1971, Distinct Element Models of rock and soil structure. In: Analytical and Computational Methods in Engineering Rock Mechanics (Ed. by E.T. Brown): Unwin Publishers, London, p. 129-163.

Cundall, P. A., and Strack, O. D. L., 1979, A discrete numerical model for granular assemblies: Géotechnique, v. 29, no. 1, p. 47-65.

D'Addetta, G. A., 2004, Discrete Models for Cohesive Frictional Materials [PhD: University of Stuttgart.

Faulkner, D. R., Jackson, C. A. L., Lunn, R. J., Schlische, R. W., Shipton, Z. K., Wibberley, C. A. J., and Withjack, M. O., 2010, A review of recent developments concerning the structure, mechanics and fluid flow properties of fault zones: Journal of Structural Geology, v. 32, no. 11, p. 1557-1575.

Finch, E., Hardy, S., and Gawthorpe, R., 2004, Discrete-element modelling of extensional fault-propagation folding above rigid basement fault blocks: Basin Research, v. 16, no. 4, p. 467-488.

Gray, G. G., Morgan, J. K., and Sanz, P. F., 2014, Overview of continuum and particle dynamics methods for mechanical modeling of contractional geologic structures: Journal of Structural Geology, v. 59, p. 19-36.

Hardy, S., 2011, Cover deformation above steep, basement normal faults: Insights from 2D discrete element modeling: Marine and Petroleum Geology, v. 28, no. 5, p. 966-972.

Hardy, S., and Finch, E., 2005, Discrete-element modelling of detachment folding: Basin Research, v. 17, no. 4, p. 507-520.

Hardy, S., McClay, K., and Anton Muñoz, J., 2009, Deformation and fault activity in space and time in high-resolution numerical models of doubly vergent thrust wedges: Marine and Petroleum Geology, v. 26, no. 2, p. 232-248.

Hart, R. D., 1988, An overview of methods for discontinuum analysis.

Jackson, C. A. L., and Lewis, M. M., 2016, Structural style and evolution of a salt-influenced rift basin margin; the impact of variations in salt composition and the role of polyphase extension: Basin Research, v. 28, no. 1, p. 81-102.

Johnson, K. M., and Johnson, A. M., 2002, Mechanical analysis of the geometry of forced-folds: Journal of Structural Geology, v. 24, no. 3, p. 401-410.

Khalil, S. M., and McClay, K. R., 2002, Extensional fault-related folding, northwestern Red Sea, Egypt: Journal of Structural Geology, v. 24, no. 4, p. 743-762.

Kuhn, M. R., 1999, Structured deformation in granular materials: Mechanics of Materials, v. 31, no. 6, p. 407-429.

Lewis, M. M., Jackson, C. A. L., and Gawthorpe, R. L., 2013, Salt-influenced normal fault growth and forced folding: The Stavanger Fault System, North Sea: Journal of Structural Geology, v. 54, p. 156-173.

Paul, D., and Mitra, S., 2015, Fault patterns associated with extensional fault-propagation folding: Marine and Petroleum Geology, v. 67, p. 120-143.

Rowan, M. G., Peel, F. J., and Vendeville, B. C., 2004, Gravity-driven fold belts on passive margins.

Sharp, I. R., Gawthorpe, R. L., Underhill, J. R., and Gupta, S., 2000, Fault-propagation folding in extensional settings: examples of structural style and synrift sedimentary response from the Suez rift, Sinai, Egypt: Geological Society of America Bulletin, v. 112, no. 12, p. 1877-1899.

Stearns, D. W., 1978, Faulting and forced folding in the Rocky Mountains foreland: Geological Society of America Memoirs, v. 151, p. 1-38.

Vendeville, B., Ge, H., and Jackson, M., 1995, Scale models of salt tectonics during basement-involved extension: Petroleum Geoscience, v. 1, no. 2, p. 179-183.

Withjack, M. O., and Callaway, S., 2000, Active normal faulting beneath a salt layer: An experimental study of deformation patterns in the cover sequence: AAPG Bulletin, v. 84, no. 5, p. 627-651.